

Dynamics of Orbits Close to Asteroid 4179 Toutatis

D.J. Scheeres

Jet Propulsion Laboratory

California Institute of Technology

Pasadena, CA

E-Mail: dan.scheeres@zeus.jpl.nasa.gov

S.J. Ostro

Jet Propulsion Laboratory

California Institute of Technology

E-Mail: ostro@echo.jpl.nasa.gov

R.S. Hudson

Washington State University

E-Mail: hudson@eecs.wsu.edu

E.M. DeJong

Jet Propulsion Laboratory

California Institute of Technology

S. Suzuki

Jet Propulsion Laboratory

California Institute of Technology

45 Manuscript pages (double spaced)

20 Numbered Figures

Proposed running title: Orbit dynamics about 4179 Toutatis

D.J. Scheeres

Before August 1, 1997:

MS 301-125J

Jet Propulsion Laboratory

California Institute of Technology

Pasadena, CA 91109-8099

E-Mail: dan.scheeres@zeus.jpl.nasa.gov

Phone: (818) 354-7128

Fax: (818) 393-6388

After August 1, 1997:

304 Town Engineering

Department of Aerospace Engineering and Engineering Mechanics

Iowa State University

Ames, Iowa 50011

E-Mail: dan.scheeres@zeus.jpl.nasa.gov

Phone: (515) 294-3776

Fax: (515) 294-3262

Abstract

We use a radar-derived physical model of 4179 Toutatis (Hudson and Ostro 1995, Science 270, 84-86) to investigate close-orbit dynamics around that irregularly shaped, non-principal-axis rotator. The orbital dynamics about this body are markedly different than the dynamics about uniformly rotating asteroids. The results of this paper have a wider application to orbit dynamics about bodies in a non-principal-axis rotation state. The radar results support the hypothesis that Toutatis has a homogeneous density distribution, and we assume a density of 2.5 g/cc. The asteroid's gravity field is computed using a truncated harmonic expansion when outside of its circumscribing sphere and a closed-form expression for the potential field of an arbitrary polyhedron when inside that sphere. The complete equations of motion are time-periodic due to the complex rotation of the asteroid. The system is Hamiltonian and has all the characteristics of such a system, including conservation of phase volume, but there is no Jacobi constant of the motion and zero velocity surfaces cannot be used to analyze the system's behavior. We also examine some of the close-orbit dynamics with the Lagrange planetary form of the equations of motion. Families of quasi-periodic "frozen orbits" that show minimal variations in orbital elements are found to exist very close to the asteroid; some of them are stable and hence can hold natural or artificial satellites. A retrograde family of frozen orbits is especially robust and persists down to semi-major axes of about 2.5 km, comparable to half of Toutatis' longest dimension. We identify families of periodic orbits, which repeat in the Toutatis-fixed frame. Due to the time-periodic nature of the equations of motion, all periodic orbits about Toutatis must be commensurate with the 5.42 day period associated with those equations. Exact calculation of both stable and unstable periodic orbits are made. The sum of surface forces acting on a particle on Toutatis is time-varying, so particles on and in the asteroid are being continually

shaken with a period of 5.42 days, perhaps enhancing the uniformity of the regolith distribution. A global map of the gravitational slope reveals that it is surprisingly shallow for such an elongated, irregularly shaped object, averaging 16° globally and less than 35° over 96% of the surface. A global map of tangential accelerations shows no values larger than 0.5 mm/s^2 , an average value of 0.2 mm/s^2 and less than 0.25 mm/s^2 over 70% of the surface. A global map of the escape speed for launch normal to the surface shows that quantity to be between 1.2 and 1.8 m/s over most of the surface. Each of these mapped quantities has small periodic variations. We have found trajectories that leave the surface, persist in the region of phase space around a frozen orbit, and then impact the surface after a flight time of more than a hundred days. Return orbit durations of years seem possible. Whereas a uniformly rotating asteroid preferentially accumulates non-escaping ejecta on its leading sides, Toutatis accumulates ejecta uniformly over its surface. We render a variety of close orbits in inertial and body-fixed frames.

Contents

1	Introduction	6
2	Toutatis Model, Rotational State and Gravity Field	6
2.1	Rotational State	8
2.2	Symmetric Inertia Tensor Approximation	12
2.3	Solar Perturbations	12
3	Equations of Motion	13
3.1	Complete Equations of Motion	13
3.2	Approximate Equations of Motion	14
4	Orbital Dynamics About Toutatis	18
4.1	The Effect of the C_{20} Gravity Term	19
4.1.1	Frozen Orbits Including Only C_{20}	21
4.2	Combined Effects of the C_{20} and C_{30} Terms	24
4.2.1	Frozen Orbits Including C_{20} and C_{30}	25
4.3	Orbits in the Full Problem	26
4.3.1	Fully Frozen Orbits in the Full Equations of Motion	28
4.3.2	Partially Frozen Orbits in the Full Equations of Motion	29
4.4	Periodic Orbits	31
4.5	Implications of the Rotational State on the Gravity Field	35
5	Dynamics of Surface Particles	37
5.1	Surface Forces	37
5.2	Surface Escape Speed	39
5.3	Dynamics of Ejected Particles	40
5.4	Distribution of Returning Ejecta	42

1 Introduction

The dynamics of orbits close to small, irregularly shaped asteroids are fundamental to studies of retention and redistribution of impact ejecta, to questions about plausible origins and lifetimes of asteroidal satellites, and to the design of robotic and piloted spacecraft missions. Scheeres et al., (1996) reviewed the literature relevant to this topic and used a radar-derived model of 4769 Castalia (Hudson and Ostro, 1994) to study close orbits around that 1.6-km-long object, whose 4.1-h principal-axis spin state is fairly ordinary.

Here we use a radar-derived model of 4179 Toutatis, a 4.6-km-long object in an unusually slow, rather complex non-principal-axis spin state. We find the close-orbit dynamics around Toutatis to be significantly different than those around a principal-axis rotator. The analysis tools developed here are generally applicable to any non-principal-axis rotator.

2 Toutatis Model, Rotational State and Gravity Field

Our physical model of Toutatis' shape and spin state was derived by Hudson and Ostro (1995) from a low-resolution subset of radar delay-Doppler images obtained in Dec. 1992 by Ostro et al. (1995). The modeling inversion solved for the asteroid's shape and inertia tensor, their orientation with respect to each other, initial conditions for the asteroid's spin and orientation, the radar scattering properties of the surface, and the projected location of the asteroid's center of mass in each frame. The model has 1600 shape parameters and an effective spatial resolution of 84 meters.

The orientational coverage provided by the combination of Toutatis' sky motion during the 18-day imaging sequence and its non-principal-axis rotation permitted the entire surface to be imaged, which in turn produced a very accurate shape model to be constructed, independent of the estimation of the inertia tensor. The modeling established that either Toutatis is nearly homogeneous or its

inhomogeneities mimic the inertia tensor of a homogeneous body. In this paper, we assume that Toutatis is homogeneous, with a density 2.5 g/cc. That value, although arbitrary, is comparable to constraints on the surface or bulk densities of other asteroids that share Toutatis' S classification: 253 Ida (bulk density = 2.6 ± 0.5 g/cc, Belton et al. 1995; 4169 Castalia surface density = 2.1 ± 0.4 g/cc, Scheeres et al. 1996; 1620 Geographos, surface density ~ 2.4 g/cc, Ostro et al. 1996)

Figure 1: Radius contours of Toutatis.

Figure 2: The shape of Toutatis and its coordinate axes shown rendered in four perspective views.

For describing positions about Toutatis we use a body-fixed coordinate system whose origin is at the model's centroid and whose axes (x, y, z) correspond to the principal axes of smallest, intermediate and largest moment of inertia, respectively. Thus the x -axis is aligned with the long axis and the z -axis is aligned with the short axis of Toutatis. Toutatis fits into the bounding box $-2.516 \leq x \leq 2.086$, $-1.174 \leq y \leq 1.116$, $-0.950 \leq z \leq 0.980$, it has a volume of 7.670 km^3 and a mean radius of 1.223 km. The ratios of the moments of inertia are:

$$I_x/I_z = 0.31335 \quad (1)$$

$$I_y/I_z = 0.94471 \quad (2)$$

Our assumed density gives a total mass of

$$M = 1.917 \times 10^{13} \text{ kg} \quad (3)$$

and a gravitational parameter

$$\mu = GM = 1.279 \times 10^{-6} \text{ km}^3/\text{s}^2 \quad (4)$$

where $G = 6.67259 \times 10^{-20} \text{ km}^3/\text{kg/s}^2$.

The most important terms of the harmonic expansion of the gravity field correspond to the C_{20} , C_{22} and C_{30} coefficients (see Kaula, 1966 for a description of gravity harmonics). For the Toutatis model these are:

$$C_{20} = 0.77768/r_o^2 \quad (5)$$

$$C_{22} = -0.01634/r_o^2 \quad (6)$$

$$C_{30} = -0.48580/r_o^3 \quad (7)$$

where r_o is an arbitrary normalization radius. These coefficients are evaluated using a coordinate frame that places the equator in the y - z plane and the “pole” along the x -axis. The gravity field involving only these terms is:

$$\begin{aligned} U = & \frac{\mu}{r} + \frac{\mu r_o^2 C_{20}}{2r^3} (3 \sin^2 \delta - 1) + \frac{3\mu r_o^2 C_{22}}{r^3} \cos^2 \delta \cos(2\lambda) \\ & + \frac{\mu r_o^3 C_{30} \sin \delta}{2r^4} (5 \sin^2 \delta - 3) \end{aligned} \quad (8)$$

where r is the particle radius measured from the body center of mass, δ is the declination of the particle and λ is the particle longitude in the body-fixed space. Note that this formulation assumes that the coordinate frame is aligned with the principal axes and that the declination is measured with respect to the minimum moment of inertia axis.

The computations used in this paper use gravitational coefficients up to order 20 when outside of the circumscribing sphere of the body (which is more than adequate). When within this sphere the gravity field is evaluated from the polyhedral shape itself (Werner 1994, Werner and Scheeres 1996).

2.1 Rotational State

Toutatis is in an unforced (torque-free), non-principal-axis (NPA) spin state. Its rotational dynamics can be described in terms of analytic functions and simple geometry (MacMillan 1960), as follows.

The (Euler) equations of motion are

$$\mathbf{I} \cdot \dot{\boldsymbol{\Omega}} = -\boldsymbol{\Omega} \times \mathbf{I} \cdot \boldsymbol{\Omega} \quad (9)$$

where \mathbf{I} is the inertia dyad of the body and $\boldsymbol{\Omega}$ is the rotational velocity vector, or instantaneous spin vector. There are two integrals for this equation, conservation of energy and conservation of angular momentum, so these equations are integrable and their solution can be expressed in terms of the fundamental constants of rotational motion:

$$\omega_l = \frac{\boldsymbol{\Omega} \cdot \mathbf{I} \cdot \boldsymbol{\Omega}}{|\mathbf{I} \cdot \boldsymbol{\Omega}|} \quad (10)$$

$$I_D = \frac{\boldsymbol{\Omega} \cdot \mathbf{I} \cdot \mathbf{I} \cdot \boldsymbol{\Omega}}{\boldsymbol{\Omega} \cdot \mathbf{I} \cdot \boldsymbol{\Omega}} \quad (11)$$

The final constant of motion describes the time at which the initial rotational vector is specified.

The constants ω_l and I_D have physical interpretations in terms of the kinetic energy

$$T = \frac{1}{2} \boldsymbol{\Omega} \cdot \mathbf{I} \cdot \boldsymbol{\Omega} \quad (12)$$

$$= \frac{1}{2} I_D \omega_l^2 \quad (13)$$

and the angular momentum magnitude

$$|\mathbf{H}| = |\boldsymbol{\Omega} \cdot \mathbf{I}| \quad (14)$$

$$= I_D \omega_l \quad (15)$$

Thus ω_l and I_D represent scalar versions of the body's effective rotation rate and inertia.

Using these integration constants the angular velocity Ω is computed as:

$$\Omega = \omega_l \begin{bmatrix} \sqrt{\frac{I_D(I_z - I_D)}{I_x(I_z - I_x)}} \operatorname{dn}(\tau - \tau_o) \\ \sqrt{\frac{I_D(I_D - I_x)}{I_y(I_y - I_x)}} \operatorname{sn}(\tau - \tau_o) \\ \sqrt{\frac{I_D(I_D - I_x)}{I_x(I_z - I_x)}} \operatorname{cn}(\tau - \tau_o) \end{bmatrix} \quad (16)$$

$$\tau - \tau_o = \sqrt{\frac{I_D(I_z - I_D)(I_y - I_x)}{I_x I_y I_z}} \omega_l (t - t_o) \quad (17)$$

where I_x , I_y and I_z are the principal moments of inertia of Toutatis, τ_o is the final constant of integration and t is time. The functions sn , cn , dn are elliptic functions and are described in MacMillan (1960) and Whittaker and Watson (1952). Toutatis is rotating about its longest axis (x), which has the minimum moment of inertia I_x .

The values of the integration constants (Hudson and Ostro, 1995) are: $\omega_l = 1.8548 \times 10^{-5}$ rad/sec corresponding to a period of 3.92 days, and $I_D = 0.51983I_z$, where I_z is used to scale all the inertia terms.

The angular velocity vector of Toutatis varies periodically with time. Within one orbit of this vector its magnitude varies between 2.1287×10^{-5} and 2.1122×10^{-5} radians/second (4.39 and 4.36 degrees/hour). Similarly, the angle between the rotational velocity vector and the x -axis varies between 21.904 and 20.162 degrees, and the angle between its x -axis and the angular momentum vector varies between 50.486 to 49.550 degrees. The period of the rotational velocity in the body-fixed frame is 130.156 hours, or 5.42 days.

For describing the orientation of Toutatis in inertial space we use the right ascension α , the declination δ and the hour angle W . The transformation matrix from the inertial frame with z -axis

along the angular momentum vector to the body-fixed frame is:

$$T = \begin{bmatrix} \cos \delta \cos \alpha & \cos \delta \sin \alpha & \sin \delta \\ -\cos W \sin \delta \cos \alpha & -\cos W \sin \delta \sin \alpha & \cos W \cos \delta \\ +\sin W \sin \alpha & -\sin W \cos \alpha & \\ \sin W \sin \delta \cos \alpha & \sin W \sin \delta \sin \alpha & -\sin W \cos \delta \\ +\cos W \sin \alpha & -\cos W \cos \alpha & \end{bmatrix} \quad (18)$$

For the Toutatis rotation state the Euler angles are computed from:

$$\cot W = \sqrt{1+n} \frac{\operatorname{sn}(\tau)}{-\operatorname{cn}(\tau)} \quad (19)$$

$$\sin \delta = \sqrt{\frac{I_z (I_z - I_D)}{I_D (I_z - I_x)}} \operatorname{dn}(\tau) \quad (20)$$

$$\alpha = \alpha_o + \frac{I_D \omega_l}{I_z} (t - t_o) - \sqrt{\frac{I_D I_y}{I_z I_x}} \frac{(I_z - I_x)}{\sqrt{(I_z - I_D)(I_y - I_x)}} [\bar{\Pi}(\tau, n, k) - \bar{\Pi}(\tau_o, n, k)] \quad (21)$$

$$n = \frac{I_x (I_z - I_y)}{I_z (I_y - I_x)} \quad (22)$$

$$k^2 = \frac{(I_D - I_x)(I_z - I_y)}{(I_y - I_x)(I_z - I_D)} \quad (23)$$

where $n = 0.02744$ and $k^2 = 0.0376$

For this rotational mode the right ascension α and hour angle W have a steady increase and the declination δ librates about a value close to 40° . The function Π is the elliptic integral of the 3rd kind and is defined as:

$$\Pi(\tau, n) = \int_0^\tau \frac{d\tau}{1 + n \operatorname{sn}^2(\tau)} \quad (24)$$

See Whittaker and Watson (1952) for a comprehensive discussion of elliptic functions and integrals.

The hour angle W describes the asteroid's roll around its x -axis, while the right ascension α describes the angle that the asteroid x -axis sweeps out in inertial space. The period of the right ascension is clearly visible when viewed from inertial space and is equal to 176.4 hours, or 7.35 days. This is also the rotation period which the asteroid would have if it relaxed its rotation from its current state to principal axis rotation about its largest moment of inertia (I_z), keeping angular momentum conserved and decreasing kinetic energy to its minimum value (as would happen in a dissipative system).

2.2 Symmetric Inertia Tensor Approximation

There is a simple approximation to the Toutatis rotation state which allows for a simplified analytical approach to solving the dynamical equations for a particle in orbit about Toutatis. There is a small total variation in nutation angle (about 0.94 degrees), but in some situations we can assume that this variation is zero. This is equivalent to assuming that the I_y and I_z principal inertia values are equal. In this case the elliptic functions $\text{sn}(\tau)$, $\text{cn}(\tau)$ and $\text{dn}(\tau)$ degenerate to $\sin(\tau)$, $\cos(\tau)$ and 1, respectively; and the asteroid rotates as if it were rolling on a circular cone; the declination δ becomes a constant and the right ascension α increases linearly with time, its period being the inertial period of the asteroid, 7.35 days; and the hour angle W also increases linearly with time. We use this approximation when analyzing the averaged equations of motion, as explained in the next section, but not when dealing with numerical solutions under the influence of the full gravitational field.

2.3 Solar Perturbations

An orbiting particle will be subject to perturbations from the sun. For an ideal point this perturbation is due solely to the solar tide, and for an extended body such as a spacecraft this perturbation will also arise from the solar radiation pressure acting on the body. Scheeres (1994b) discusses these effects in greater detail for a spacecraft. The effect of solar radiation pressure is not treated at all

in this paper, while we will give a few comments on the effect of the solar tide.

The semi-major axis and eccentricity of Toutatis are 2.5154 AU and 0.6362, leading to perihelion and aphelion distances of 0.915 and 4.116 AU. Combining these with the assumed Toutatis gravitational parameter ($1.279 \times 10^{-6} \text{ km}^3/\text{s}^2$) we find that the Sun-Toutatis libration points will vary from ~ 170 km at perihelion to ~ 1260 km at aphelion. Applying results from Hamilton and Burns (1991) to Toutatis we find that orbits within ~ 85 km will remain bound to Toutatis over long time periods. In Scheeres (1994b) the effect of the solar tide on an asteroid orbiter is characterized and compared to the effect of the oblateness of the body. Applying the results of that paper we find the effects of Toutatis' oblateness and of the solar tide on a particle orbit are equal at a semi-major axis of ~ 30 km at perihelion and ~ 99 km at aphelion. Both effects are quite small at these radii, while the effect of the solar tide increases with increasing semi-major axis and that of the oblateness decreases with increasing semi-major axis. For the orbital situations discussed in this paper the effect of the solar tide will be relevant only when Toutatis is near perihelion, and even then it will be a such a small effect that we ignore it.

3 Equations of Motion

To study the dynamics of a particle in the Toutatis system one must study solutions to the equations of motion. These equations are well defined functions of Toutatis's gravity field and spin state, and are suited for full numerical integrations of close orbits. However, it is also instructive to introduce approximate equations of motion that can simplify some analyses and shed light on the character of the dynamics.

3.1 Complete Equations of Motion

To describe motion about Toutatis in the most complete sense, we write the equations of motion of a particle in a body-fixed coordinate system:

$$\ddot{\mathbf{r}} + 2\dot{\boldsymbol{\Omega}} \times \dot{\mathbf{r}} + \boldsymbol{\Omega} \times (\boldsymbol{\Omega} \times \mathbf{r}) + \dot{\boldsymbol{\Omega}} \times \mathbf{r} = \mathbf{U}_r \quad (25)$$

where \mathbf{r} is the body-fixed vector from the asteroid center of mass, $(\dot{})$ and $(\ddot{})$ are first and second time derivatives with respect to the body-fixed, rotating frame, $\boldsymbol{\Omega}$ is the instantaneous rotation vector of the asteroid and $U_{\mathbf{r}}$ is the gradient of the gravitational potential $U(\mathbf{r})$, which is time-invariant in the Toutatis-fixed frame.

As the rotational velocity vector $\boldsymbol{\Omega}$ can be expressed in terms of analytic equations, the equations of motion can be evaluated as an analytic function of time. These equations of motion are time-periodic as the rotational velocity is periodic with period 5.42 days. To evaluate the term $\dot{\boldsymbol{\Omega}}$ in the equations use Eq. (9). In this complete system, we will always include the full rotational dynamics without any approximation and will use the full gravity field.

There is a rich literature on the properties of solutions of time-periodic equations of motion, and some very general results can be stated about the properties of solutions to these equations. For the current analysis, there are several points that are helpful to make. First, the Jacobi integral does not exist for this system. Second, despite this these equations still describe a general Hamiltonian system, so the integral invariants will all exist; namely the divergence of the equations is zero so that these equations still conserve phase volume. This point is very important when we consider the stability of solutions to the complete equations, as the invariance of phase volume implies that no solution to these equations can be asymptotically stable. It is this general property of Hamiltonian systems that make long-term dynamical predictions very difficult. Third, any periodic solution of these equations must have a period which is an integral multiple of the period of the equations of motion, 5.42 days, in contrast with the case of a uniformly rotating body (Scheeres, 1994a, Scheeres et al., 1996) for which periodic orbits exist over a continuous range of periods.

3.2 Approximate Equations of Motion

To enable analytical solutions of the equations of motion it is usually required to simplify them to a form that is more amenable to analysis and to qualitative understanding. Before simplifying the equations of motion, it is convenient to cast them into the Lagrange planetary equations (Brouwer

and Clemence, 1961). Given a perturbing potential of the form R , these equations are:

$$\frac{da}{dt} = \frac{2}{na} \frac{\partial R}{\partial M_o} \quad (26)$$

$$\frac{de}{dt} = \frac{1-e^2}{na^2 e} \frac{\partial R}{\partial M_o} - \frac{\sqrt{1-e^2}}{na^2 e} \frac{\partial R}{\partial \omega} \quad (27)$$

$$\frac{di}{dt} = \frac{\cot(i)}{na^2 \sqrt{1-e^2}} \frac{\partial R}{\partial \omega} - \frac{\csc(i)}{na^2 \sqrt{1-e^2}} \frac{\partial R}{\partial \Omega} \quad (28)$$

$$\frac{dM_o}{dt} = -\frac{2}{na} \frac{\partial R}{\partial a} - \frac{1-e^2}{na^2 e} \frac{\partial R}{\partial e} \quad (29)$$

$$\frac{d\omega}{dt} = \frac{\sqrt{1-e^2}}{na^2 e} \frac{\partial R}{\partial e} - \frac{\cot(i)}{na^2 \sqrt{1-e^2}} \frac{\partial R}{\partial i} \quad (30)$$

$$\frac{d\Omega}{dt} = \frac{\csc(i)}{na^2 \sqrt{1-e^2}} \frac{\partial R}{\partial i} \quad (31)$$

where a is the semi-major axis, e is the eccentricity, i is the inclination, ω is the argument of periapsis, Ω is the argument of the ascending node, M_o is the mean anomaly epoch and n is the mean motion. Unlike the complete formulation, which was expressed in the Toutatis fixed frame, this simplified formulation is made in the inertial frame. Thus, the perturbing potential R (which equals the full gravity field minus the central potential $\mu/|\mathbf{r}|$) must include the rotational dynamics of Toutatis implicitly.

In this paper we will concentrate on the gravity coefficients C_{20} and C_{30} , which control the majority of the qualitative dynamics seen about Toutatis. Unlike uniformly rotating asteroids (Scheeres, 1996) the effects associated with the C_{22} term do not play a large role at Toutatis for reasons which will be discussed.

In the following discussion the inclination of the orbit and the “equatorial” plane are defined by the Toutatis rotational angular momentum vector, which is assumed to be fixed in inertial space. To describe Toutatis’ inertial orientation it is sufficient to express the unit vector of Toutatis’s x -axis

in inertial coordinates:

$$P_z = [\cos \delta \cos \alpha, \cos \delta \sin \alpha, \sin \delta] \quad (32)$$

where δ and α are Euler angles. In general P_z will rotate about the z -axis and nutate, as δ librates in the vicinity of 40° and α increases with time. However if we invoke the symmetric inertia tensor approximation then $\delta = 40^\circ$ constant, and $\alpha = \dot{\alpha}t$ with a period of 7.35 days.

It is also necessary to specify the particle orbit in inertial space. Given an inertial coordinate frame with \hat{z} along the asteroid's rotational angular momentum vector, define the vectors:

$$r_h = \sin \Omega \sin i \hat{x} - \cos \Omega \sin i \hat{y} + \cos i \hat{z} \quad (33)$$

$$r_T = -\sin \Omega \cos i \hat{x} + \cos \Omega \cos i \hat{y} + \sin i \hat{z} \quad (34)$$

$$r_\Omega = \cos \Omega \hat{x} + \sin \Omega \hat{y} \quad (35)$$

where Ω is the argument of the ascending node and i is the inclination. r_h is the unit vector along the orbit's angular momentum vector, r_Ω defines the location of the ascending node in the $\hat{x} - \hat{y}$ plane, and r_T completes the orthogonal set. Using these vectors the position vector of the orbiting particle is:

$$r = r [\cos u r_\Omega + \sin u r_T] \quad (36)$$

where r is the radius of the particle and $u = f + \omega$, where f is the true anomaly and ω is the argument of the periapsis.

Given these definitions the contributions of C_{20} and C_{30} to the gravity field are:

$$R_{20} = \frac{\mu C_{20}}{2r^3} [3(P_z \cdot r_s)^2 - 1] \quad (37)$$

$$R_{30} = \frac{\mu C_{30}(P_z \cdot r_s)}{2r^4} [5(P_z \cdot r_s)^2 - 3] \quad (38)$$

where \mathbf{r}_s is the unit vector pointing towards the particle ($\mathbf{r}_s = \cos u \mathbf{r}_\Omega + \sin u \mathbf{r}_T$).

The influence of the C_{20} and C_{30} terms on Toutatis's close-orbit dynamics becomes clear if we average the Lagrange planetary equations. The usual practice is to average over one orbit of the particle, but in some situations it is useful to average over the (time-varying) potential as well.

Under the symmetric inertia tensor approximation, Toutatis's x -axis rotates once around the angular momentum vector every 7.35 days. A particle orbit's period, to first approximation, is:

$$T \sim \frac{2\pi}{\sqrt{\mu}} a^{3/2} \quad (39)$$

$$1.543 a^{3/2} \text{ hours} \quad (40)$$

where the semi-major axis a is expressed in kilometers. Thus, these two periods are equal when $a = 23.55$ km. The averaging procedure is not strictly valid around this resonance, but further from the asteroid it is acceptable to average over both the particle orbit and Toutatis's rotational motion. Since the orbit perturbations due to Toutatis are so small at these distances, we do not discuss the regimes outside of 20 km. Figure 3 shows the number of Toutatis revolutions per particle orbit as a function of semi-major axis.

Figure 3: Number of Toutatis revolutions per particle orbit. Three regimes are identified here, the sub-resonant regime where the particle has multiple orbits per Toutatis rotation, the resonant regime where the orbit and Toutatis period are approximately equal, and the super-resonant regime where Toutatis has multiple rotations per particle orbit.

Holding the Toutatis rotation state fixed and averaging the perturbing potentials over one particle orbit yields:

$$\bar{R}_{20} = \frac{n^2 C_{20}}{4(1-e^2)^{3/2}} [1 - 3(\mathbf{P}_x \cdot \mathbf{r}_h)^2] \quad (41)$$

$$\bar{R}_{30} = \frac{3en^2C_{30}}{8a(1-e^2)^{5/2}} (1 - 5(P_z \cdot r_h)^2) [(P_z \cdot r_\Omega) \cos \omega + (P_z \cdot r_T) \sin \omega] \quad (42)$$

where:

$$P_z \cdot r_h = \cos i \sin \delta + \sin i \cos \delta \sin \lambda \quad (43)$$

$$P_z \cdot r_\Omega = \cos \delta \cos \lambda \quad (44)$$

$$P_z \cdot r_T = \sin i \sin \delta - \cos i \cos \delta \sin \lambda \quad (45)$$

In these equations i is the inclination and λ is the relative node where $\lambda = \Omega - \alpha$. These averaged potentials can then be used in the Lagrange equations with the Euler angles as a function of time. Note that there is no need to restrict the above potential to the symmetric inertia tensor approximation, although below we do this to analyze the dynamics using these averaged potentials.

Now, for completeness, we average over the Toutatis rotational dynamics as well. We adopt the symmetric inertia tensor approximation, so the declination δ is fixed and α increases linearly in time. Introducing these assumptions and averaging over time yields the doubly-averaged potential:

$$\bar{R}_{20} = \frac{\mu C_{20}}{4a^3(1-e^2)^{3/2}} \left[1 - \frac{3}{2} \cos^2 \delta \sin^2 i - 3 \cos^2 i \sin^2 \delta \right] \quad (46)$$

We do not compute the second average of R_{30} as it has a negligible effect at these larger radii.

Note that if $\delta \rightarrow 90^\circ$, then the potential \bar{R}_{20} becomes equivalent to the familiar averaged potential for an oblate/prolate body. Thus, motion in the super-resonant regime will be similar to the familiar case of orbiting a body with rotational symmetry about its spin axis.

4 Orbital Dynamics About Toutatis

In this section we proceed from the simplified system to the complete system, starting with discussion of the averaged effect of the C_{20} gravity term. In conjunction with this term we will find a family of “frozen orbits” defined for a wide range of orbital parameters. Study of these orbits and the

simplified equations will shed light on some general results for orbits about a body in complex rotation. Next, the effect of the C_{30} gravity term will be added and its influence for Toutatis orbits will be discussed. A more restricted class of frozen orbits is defined even when this effect is included. Finally, motion in this regime under the full equations of motion, with no rotational or gravitational approximations, is discussed. Again, subsets of the families of frozen orbits found in the simplified systems persist even in this more dynamic environment.

A “frozen orbit” is not a periodic orbit – it does not necessarily close upon itself in phase space. Rather, an orbit is considered to be frozen when its averaged orbital elements, or some function of its averaged orbital elements, are constant solutions to the averaged equations of motion. If a frozen orbit is stable and its initial conditions are used in the non-averaged equations of motion, then the osculating orbital elements in the ensuing motion will oscillate about the values corresponding to the frozen orbit, so frozen orbits are more easily identified with quasi-periodic orbits than with periodic orbits themselves. The stability of a frozen orbit is usually evaluated in terms of the averaged equations themselves, so frozen orbit stability is no guarantee that motion in the full system will oscillate about the frozen orbit elements. Indeed, if the transient variations in the full system are too large, the averaging assumption may no longer apply and the frozen orbits may not persist in the full system. Conversely, if the transient variations are small enough, or the frozen orbit stability robust enough, then the frozen orbit may persist in the full system and can be identified as a class of orbits that yield minimal variations in the orbital elements. Such classes of orbits are useful in analyzing the phase space of a system and, practically, are candidate orbits for natural and artificial satellites.

4.1 The Effect of the C_{20} Gravity Term

Considering only the C_{20} gravity term in the averaged Lagrange equations we find:

$$\frac{da}{dt} = 0 \quad (47)$$

$$\frac{de}{dt} = 0 \quad (48)$$

$$\frac{di}{dt} = \frac{3nC_{20}}{2p^2} (P_x \cdot r_h)(P_x \cdot r_\Omega) \quad (49)$$

$$\frac{d\lambda}{dt} = \frac{3nC_{20}}{2p^2} \csc i (P_x \cdot r_h)(P_x \cdot r_T) - \dot{\alpha} \quad (50)$$

$$\frac{d\omega}{dt} = \frac{3nC_{20}}{4p^2} [1 - 3(P_x \cdot r_h)^2] - \frac{3nC_{20}}{2p^2} \cot i (P_x \cdot r_h)(P_x \cdot r_T) \quad (51)$$

$$\frac{dM_o}{dt} = \frac{3nC_{20}}{4p^2} \sqrt{1 - e^2} [1 - 3(P_x \cdot r_h)^2] \quad (52)$$

Invoking the symmetric inertia-tensor approximation, we assume that $\dot{\alpha}$ is constant and that the declination $\delta = 40^\circ$ and is constant. The dynamics of i and λ are coupled only with each other and the dynamics of ω are coupled to the dynamics of these two elements. The evolution of i and λ exhibit periodic motion and appear to be integrable in a formal sense. The dynamics of M_o feed directly into all of these equations as it implies a modification of the semi-major axis a . Given an initial semi-major axis of a , the motion of the epoch modifies it to:

$$\bar{a} = \frac{a}{(1 + M_o/n)^{2/3}} \quad (53)$$

In computing values and conditions from the Lagrange equations, \bar{a} should replace a everywhere, and the above equation can then be used to recover the true value of a .

The magnitude of the orbit angular momentum vector is conserved in this system because both a and e are conserved. The orbit angular momentum unit vector, however, is not conserved and will precess and nutate as a function of time. Note that the projection of the instantaneous change in the angular momentum vector is perpendicular to the asteroid pole, P_x , i.e., that $P_x \cdot \dot{r}_h = 0$.

4.1.1 Frozen Orbits Including Only C_{20}

When the C_{20} coefficient is studied in isolation there is a family of frozen orbits that merit some study. In the current problem the elements which can be frozen are the inclination i and node λ .

Assume that the node λ is at the value $\pm\pi/2$, then:

$$P_x \cdot r_\Omega|_{\lambda=\pm\pi/2} = 0 \quad (54)$$

$$P_x \cdot r_h|_{\lambda=\pm\pi/2} = \sin(\delta \pm i) \quad (55)$$

$$P_x \cdot r_T|_{\lambda=\pm\pi/2} = \mp \cos(\delta \pm i) \quad (56)$$

where the \pm denotes whether $\lambda = \pm\pi/2$. Inserting these values into Eqs. (49) and (50) yields:

$$\frac{di}{dt} = 0 \quad (57)$$

$$\frac{d\lambda}{dt} = \frac{3nC_{20}}{2p^2} \csc i \sin(\delta \pm i)(\mp \cos(\delta \pm i)) - \dot{\alpha} \quad (58)$$

Then if λ can be frozen both i and λ will be constant on average. The condition for λ to be frozen can be written as:

$$\mp \frac{3nC_{20}}{4p^2} \csc i \sin 2(\delta \pm i) = \dot{\alpha} \quad (59)$$

This can be converted into a condition on the semi-major axis and eccentricity:

$$a^{7/2}(1-e^2)^2 = \mp \frac{3\sqrt{\mu}C_{20}}{4\dot{\alpha}} \csc i \sin 2(\delta \pm i) \quad (60)$$

$$= \mp 66.668 \csc i \sin 2(\delta \pm i) \quad (61)$$

where the sign and corresponding value of λ are chosen so that the right-hand side of the equation is positive ($\mp \sin 2(\delta \pm i) > 0$).

From this relationship we can extract specific inclination ranges where frozen orbits will exist: $(2m+1)\pi/2 \mp \delta < i < m\pi \mp \delta$, where $m = 0, \pm 1, \pm 2, \dots$. For Toutatis, with $\delta = 40^\circ$, for the $\lambda = \pi/2$ solution the frozen inclinations lie between $50^\circ < i < 140^\circ$, while for the $\lambda = -\pi/2$ solution the possible inclinations are $0^\circ \leq i < 40^\circ$ and $180^\circ \geq i > 130^\circ$. For the nominal values of Toutatis these solutions are plotted in Figure 4 for circular orbits ($e = 0$).

Figure 4: Semi-major axis for a frozen circular orbit as a function of inclination and node λ . Derived using the averaged equations with C_{20} only.

The stability of these frozen orbits in the averaged equations of motion can also be computed by linearizing the frozen orbit solution about λ and i and noting that the linear system can be reduced to the simple equation:

$$\delta\ddot{\lambda} + A^2\delta\lambda = 0 \quad (62)$$

$$A^2 = \mp \frac{\dot{\alpha}^2 \sin i \cos \delta}{\cos(\delta \pm i)} [\cot i + \cot(\delta \pm i) - \tan(\delta \pm i)] \quad (63)$$

A solution is stable if $A^2 > 0$ and is unstable otherwise. The $\lambda = \pi/2$ solutions are unstable for $i > 93^\circ$, while all of the $\lambda = -\pi/2$ are stable. This stability criterion is a weak one at best, as in the face of the non-averaged gravity field the true solutions suffer large oscillations about the nominal frozen elements. Moreover the oscillation period associated with the linear solution tends to be long, on the order of days, so the gravity field can operate on the oscillating solution over longer time spans.

Now consider the argument of periapsis. Writing Eq. (51) at the frozen orbit condition yields:

$$\frac{d\omega}{dt} = \mp \frac{\sin i \dot{\alpha}}{\sin 2(\delta \pm i)} [1 \pm \cot i \sin 2(\delta \pm i) - 3 \sin^2(\delta \pm i)] \quad (64)$$

If i and λ are frozen, then ω will have a secular motion in general. Whenever the transcendental equation $1 \pm \cot i \sin 2(\delta \pm i) - 3 \sin^2(\delta \pm i)$ equals zero this secular rate is nominally zero. For the

$\lambda = \pi/2$ frozen orbit solution this only occurs at $i = 101.0^\circ$, which is an unstable solution (the other solutions at $i = 26.1^\circ, 152.9^\circ$ occur at non-frozen orbit values of the inclination). For the $\lambda = -\pi/2$ frozen orbit solution this occurs at $i = 27.1^\circ$ and 153.9° (the other solution at $i = 79.0^\circ$ occurs at a non-frozen orbit value of the inclination). The ability of the argument of periapsis to be frozen will be of greater interest once the C_{30} gravity field term is considered.

When near a stable frozen orbit solution the node λ will oscillate about $\pm\pi/2$ and the inclination will oscillate about a mean value close to the frozen inclination value. The argument of periapsis will in general have a secular motion, although there are special values of inclination at which this element will also be frozen, as noted above.

If not started at or near such a frozen orbit (in the case of C_{20} only) the resulting dynamics of i and λ are more complex. The motion for i exhibits, in general, a double periodicity while λ can either increase or decrease secularly or librate about a mean value. Figure 5 plots the averaged inclination and Figure 6 plots $\tan(i/2) \sin \lambda$ and $\tan(i/2) \cos \lambda$ for a sequence of orbits for a fixed initial inclination and semi-major axis with $e = 0$ as the initial value of λ is changed. These plots show the solution to the averaged equations only and thus are idealized.

Figure 5: The evolution of the inclination and relative node for different initial values of the node λ for orbits with initial values $a = 3.0, e = 0, i = 70$, which are frozen initial conditions for $\lambda = \pi/2$. Here, $\lambda = \pi/2$ yields the frozen solution while $\lambda = -\pi/2$ yields the maximum excursion in the inclination. Integrated using the averaged equations with C_{20} only.

If the orbit is not locked into a frozen orbit, then the $\dot{\alpha}$ term in the equation for $\dot{\lambda}$ may dominate the equation and the generalized node can be modeled as a monotonically decreasing element. In this case the driving equations of motion reduce to:

$$\dot{i} = \left(\frac{3nC_{20}}{4p^2} \right) (\cos^2 \delta \sin 2\lambda \sin i + \sin 2\delta \cos \lambda \cos i) \quad (65)$$

Figure 6: The evolution of the inclination and relative node for different initial values of the node λ for orbits with initial values $a = 3.3, e = 0, i = 27$, which are frozen initial conditions for $\lambda = -\pi/2$. Here, $\lambda = -\pi/2$ yields the frozen solution while $\lambda = \pi/2$ yields the maximum excursion in the inclination. Integrated using the averaged equations with C_{20} only.

$$\dot{\lambda} = -\left(\frac{3nC_{20}}{4p^2}\right) [\cos^2 \delta - 2\sin^2 \delta] \cos \bar{i} - \dot{\alpha} \quad (66)$$

where the term \bar{i} denotes the time average of the inclination used to compute the general secular trend in λ and the singly averaged potential for λ has been replaced with the doubly averaged potential. Neglecting the eccentricity variations, the equation for the evolution of inclination then takes on a simple form, being driven by time periodic amplitudes. A full solution for the inclination cannot be found in general for this case. However, solutions can be found if each driving term is considered separately and are of the form $\exp(\cos \lambda)$ and $\exp(\sin 2\lambda)$.

4.2 Combined Effects of the C_{20} and C_{30} Terms

Now consider what happens in the averaged equations when the C_{30} term is added to the dynamics. In the averaged equations the C_{30} term has no effect on the semi-major axis and has a second order effect on the inclination, relative node, argument of periapsis and the mean epoch. Thus this term acts primarily on the eccentricity, yielding the additional equation:

$$\frac{de}{dt} = \frac{3nC_{30}}{8ap^2} (1 - 5(P_z \cdot \mathbf{r}_h)^2) [(P_z \cdot \mathbf{r}_\Omega) \sin \omega - (P_z \cdot \mathbf{r}_T) \cos \omega] \quad (67)$$

This equation links the dynamics of e and ω to the previously closed system of i and λ , and thus complicates the dynamics significantly. Practically speaking, the eccentricity now has a long-period oscillation, causing the total angular momentum of the orbit to no longer be conserved and allowing the periapsis radius to descend to lower altitudes.

Whereas motion in the averaged system with only C_{20} present was seen to be regular (see Figs. 5 and 6), the C_{30} term destroys this regularity. Since the semi-major axis is conserved, the particle orbits cannot escape from Toutatis. However, due to the eccentricity oscillation the periapsis radius can be decreased to a value at which impact with Toutatis occurs. Thus, the C_{30} term is the primary mechanism by which particles are removed from orbit via impacts with the Toutatis surface. At larger orbital radii there may be enough "clearance" between the minimum periapsis radius and the asteroid surface to avoid this impact. In this case the orbits are stable in the averaged equations and can continue indefinitely.

4.2.1 Frozen Orbits Including C_{20} and C_{30}

Since we have not modified the dynamical equations for the elements other than eccentricity, the frozen orbit results discussed previously still hold. Now, evaluating Eq. (67) at a frozen orbit yields the equation:

$$\frac{de}{dt} = \pm \frac{3nC_{30}}{8ap^2} [1 - 5\sin^2(\delta \pm i)] \cos(\delta \pm i) \cos \omega \quad (68)$$

where the initial semi-major axis and eccentricity are properly chosen according to Eq. (60). The equation is multiplied by $\cos \omega$, implying that the eccentricity can be frozen if the argument of periapsis is frozen at $\pm\pi/2$. Thus, there is still the possibility of designing an orbit which is completely frozen in all of its averaged elements.

A question of immediate interest is the stability of these solutions. As discussed previously, there are only two stable solutions in the C_{20} case where the argument of periapsis is frozen; at $i = 27.1^\circ$ and $i = 153.9^\circ$ with $\lambda = -90^\circ$ and a and e chosen properly. The characteristic equation for this system (i , λ , ω and e coupled together) can be written in the form:

$$\Lambda^4 + A^2(1 - e \sin \omega C_{30} \epsilon_1) \Lambda^2 - e \sin \omega C_{30} [1 - 5\sin^2(\delta - i)] \epsilon_2 = 0 \quad (69)$$

where A^2 is the same coefficient as in Eq. (63), ϵ_1 is small relative to A^2 , $\epsilon_2 > 0$ and $\omega = \pm\pi/2$. The stability condition for this system is that all solutions Λ^2 to the above quadratic equation be

real and negative. Writing out the solution we see:

$$\Lambda^2 = -\frac{1}{2}A^2(1 - e \sin \omega C_{30} \epsilon_1) \quad (70)$$

$$\pm \frac{1}{2} \sqrt{A^4(1 - e \sin \omega C_{30} \epsilon_1)^2 + 4e \sin \omega C_{30} [1 - 5 \sin^2(\delta - i)] \epsilon_2}$$

The controlling stability condition, assuming that $\epsilon_1 \ll A^2$, is that $\sin \omega C_{30} [(1 - 5 \sin^2(\delta - i))] < 0$, as then Λ^2 is assured to be negative. For Toutatis C_{30} is negative, implying that for the $i = 27.1^\circ$ solution the $\omega = \pi/2$ frozen orbit solution is stable and the $\omega = -\pi/2$ frozen orbit solution is unstable; conversely, for the 153.9° solution the $\omega = -\pi/2$ frozen orbit solution is stable and the $\omega = \pi/2$ frozen orbit solution is unstable.

Figures 7 and 8 show the inclination and periapsis radius of the stable and unstable frozen orbits over 100 days. These runs were made by integrating the averaged equations with the initial conditions $a = 3.3, e = 0, i = 27, \lambda = -90$ and $\omega = \pm 90$ (which are slightly perturbed from a frozen orbit). The solution to the unstable system shows the large disruption that the C_{30} term can have on the orbit dynamics.

Figure 7: The evolution of the averaged inclination over 100 days starting in a frozen orbit (including a frozen argument of periapsis) with $\omega = \pm 90$. The $\omega = \pi/2$ case has a stable eccentricity variation while the $\omega = -\pi/2$ case is unstable. Integrated using the averaged equations with both C_{20} and C_{30} .

4.3 Orbits in the Full Problem

The analysis performed above using the averaged equations of motion shed light on the qualitative dynamics of motion about an asteroid such as Toutatis. Two major components to the motion are seen, due to the C_{20} term and the C_{30} term respectively. The C_{20} term causes the orbit angular

Figure 8: The evolution of the averaged periapsis radius over 100 days starting in a frozen orbit (including a frozen argument of periapsis) with $\omega = \pm 90$. The $\omega = \pi/2$ case has a stable eccentricity variation while the $\omega = -\pi/2$ case is unstable. Integrated using the averaged equations with both C_{20} and C_{30} .

momentum vector to precess and nutate while the C_{30} term causes the eccentricity to vary with time. These effects, taken either separately or together, can move an orbit's osculating elements far from their initial values. When orbits are evaluated in the full problem, including the full gravity field and the unapproximated rotational state, the motion retains the same qualitative signatures as would be expected from the averaged analysis: oscillations in the inclination and eccentricity with the semi-major axis are conserved on average. However, while the averaged equations predict the qualitative behavior of the orbit, they do not, in general, provide a precise prediction of how an individual orbit will evolve.

Now we will investigate both the fully frozen orbits (where the inclination, relative node, argument of periapsis and eccentricity are frozen) and the partially frozen orbits (where only the inclination and relative node are frozen). Since the unstable solutions will in general be unstable in the full problem as well, we investigate only those orbits that were found to be stable in the averaged approximation, aiming to answer several questions. First, do the appropriate elements oscillate about their nominally frozen values, and more specifically does the frozen orbit “persist” in the full equations of motion? By persist we mean that the orbit retains its characteristic frozen nature over a finite time interval, arbitrarily set to 50 days in this paper. Persistence of a frozen orbit solution indicates that the orbit is a stable quasi-periodic solution and may be of interest for an orbiting spacecraft. Second, if the orbit elements do not oscillate about their nominally frozen values, does the orbit still persist in that it does not impact Toutatis over the time span indicated? Orbits of this type may be chaotic and hence of interest from a dynamical systems point of view.

And lastly, if the orbit does not persist, how swiftly does it impact with the Toutatis surface? In this case the initial frozen orbit may be an unstable quasi-periodic solution which provides an indication of how long ejected particles can survive in orbit before they are swept up onto the surface again.

4.3.1 Fully Frozen Orbits in the Full Equations of Motion

Out of the six fully frozen orbits found in the previous sections only two were found to be stable in the averaged equations, both with a relative node of -90° and occurring at inclination and argument of periapsis pairs of $i = 27.1^\circ, \omega = +90^\circ$ and $i = 153.9^\circ, \omega = -90^\circ$. The first is called the direct fully frozen orbit and the latter the retrograde fully frozen orbit. For each of these the semi-major axis/eccentricity constraints are (Figure 9):

$$a^{3.5}(1 - e^2)^2 = \begin{cases} 63.695 & \text{direct} \\ 112.261 & \text{retrograde} \end{cases} \quad (71)$$

Figure 9: Semi-major axis and eccentricity relations for the direct and retrograde fully frozen orbits. The corresponding radius of periapsis is also shown. Derived using the averaged equations with both C_{20} and C_{30} .

To check the persistence of these frozen orbits, initial conditions for $e = 0, 0.1, 0.3$ and 0.5 were propagated in the full equations of motion for 50 days. All of the direct fully frozen orbits proved to be unstable and impacted with Toutatis within a few days after diverging from the initial orbital element values. Their instability can be understood if one recalls that at these values the secular rate of ω is small or zero, although the transient oscillations cause this element to vary from its initial value of 90° . This allows for a secular increase in eccentricity which leads to impact for this class of orbit. (This simple test does not preclude the possible existence of a fully frozen direct orbit in this vicinity. A higher-order analysis of the frozen orbits accounting for the transient oscillations may provide a better starting condition for the motion.)

The retrograde fully frozen orbits were also unstable (for the same reason) and eventually impacted, although some persisted for over 50 days before doing so. The longer persist times were due to the greater semi-major axis of these orbits. Curiously, if we input the same orbital parameters but shift the argument of periapsis to $+90^\circ$, then the retrograde orbits persist for arbitrary lengths of time. (These orbits appear stable but are not fully frozen in that the argument of periapsis has a secular trend and the eccentricity has large variations.)

4.3.2 Partially Frozen Orbits in the Full Equations of Motion

We also consider the evolution of the partially frozen orbits in the real model. These orbits nominally yield constant values of λ and i on average, but allow the argument of periapsis to have a secular rate and hence the eccentricity will have oscillations. These frozen orbits are more robust and are more persistent in the complete model. They have a fixed inclination with respect to the Toutatis angular momentum vector, and the orbit plane will precess around this vector with a period equal to the Toutatis period about its angular momentum vector in inertial space, approximately 7.54 days. The varying eccentricity will modify the angular momentum of the orbit and cause the secular rate of ω to vary in the orbit as well.

Let us divide these frozen orbits into three main families: direct, retrograde and positive-node partially frozen orbits (see Fig. 4). The direct and retrograde families have a relative node of -90° , and as the name indicates the positive-node family has a relative node of $+90^\circ$. As was observed before, the positive node family is only formally stable for inclinations less than 93° . All members of this family that were checked are unstable in the relative node and hence have larger variations in inclination. A few members were found that persisted for over 50 days, but none that persisted for over 100 days. Thus this partially frozen orbit family does not seem to exist in the full problem.

The direct partially frozen orbits were seen to persist for semi-major axes greater than 3.6 km (inclinations less than 24°). When at lower semi-major axes the secular rate in the argument of periapsis begins to slow and the eccentricity variations become large enough to send the orbit into impact with Toutatis. At lower semi-major axis values, where the secular rate of the argument of

periapsis grows again, this family does not reappear and remains unstable.

The family of retrograde partially frozen orbits proves to be much more robust and persists through the neighborhood of its completely frozen family member (although it does not freeze its argument of periapsis and eccentricity) down to semi-major axes of about 2.5 km. At the lower range of semi-major axis the persistence of the orbit is a function of its initial argument of periapsis. As one changes this angle (holding all other conditions fixed) the subsequent orbits will or will not persist. Therefore, the solutions are occurring in a rather sensitive area of phase space, possibly broken into regions of stable and unstable quasi-periodic orbits. The existence of stable members of this family may be related to these orbits being retrograde, as in the case of uniformly rotating asteroids one finds that retrograde orbits tend to be much more stable. The mechanism for this stability is not yet clear, but probably involves an effective averaging of the gravity field, as is the case for retrograde orbits about uniformly rotating asteroids. The persistence of these frozen orbits is remarkable in that the orbit periapsis will often dip below the maximum radius of Toutatis. Yet since the orbit plane is locked into a resonance with Toutatis, the orbit is protected from impact with the asteroid. Given that the current frozen orbit analysis does not consider the effect of the short period oscillations on the particle orbit, it is conceivable that improved initial conditions could be computed which would allow the frozen orbits to persist over a wider range of orbits. Figure 10 shows the trajectory of such an orbit in the Toutatis-fixed frame.

Figure 10: Frozen orbit plotted in the Toutatis-fixed frame over 100 days. Initial condition is a circular retrograde frozen orbit with semi-major axis of 3 km, inclination of 139° . Integrated using the full equations of motion with no approximation.

4.4 Periodic Orbits

Periodic orbits, which close on themselves in the body-fixed frame are interesting for several reasons, especially when computed using the full equations of motion. First, once a periodic orbit is found, the solution to the equations of motion is valid for all time. Second, having found such an orbit, it is then possible to compute its stability properties, which also provide insight into the stability of general motion in the phase space near the periodic orbits. For example, if a periodic orbit is found to be stable, then the region of phase space about that orbit will also be stable and will consist of quasi-periodic orbits. Conversely, if a periodic orbit is found to be unstable, then its hyperbolic manifolds will also influence motion in the surrounding phase space and cause it to be unstable as well. Unlike uniform rotators where families of periodic orbits can have arbitrary periods, periodic orbits around a complex rotator can only have periods that are commensurate with the period of the rotational velocity in the body-fixed frame (130.156 hours for Toutatis). Due to the time-periodic nature of the equations of motion in the body-fixed frame, an orbit that repeats itself with a period different than the period of the equations of motion will be subject to different accelerations and will not follow the same path.

The condition for an orbit to be periodic is:

$$\mathbf{r}(t_o) = \mathbf{r}(t_o + NT) \quad (72)$$

$$\mathbf{v}(t_o) = \mathbf{v}(t_o + NT) \quad (73)$$

where t_o is an arbitrary initial time, T is the period of the equations of motion (130.156 hours) and $N = 1, 2, 3, \dots$ is the number of periods over which the solution closes in on itself.

To compute the periodic equations in the full equations of motion one must take an initial guess of a periodic orbit and integrate it over NT , computing the state transition matrix at the same time. Then the offset between the initial and final conditions must be multiplied by the inverse of the state transition matrix so that the appropriate correction can be applied to the initial condition.

This entire process is iterated until the mis-match between the initial and final conditions is equal to zero (within the numerical accuracy of the integrator). Since there is no Jacobi integral in this problem, the state transition matrix is fully invertible. (This is not the case for uniformly rotating asteroids where the computation of periodic orbits must be made in a four-dimensional subset of the six-dimensional initial state.)

The difficulty in this computation is in finding a good initial guess to the periodic orbit, as the convergence radius in the complete equations of motion tends to be quite small. Various tricks and approximations may be used to generate the initial conditions and an approach which works uniformly well has not been found to date. An attractive, and sometimes successful, approach is to use the averaged equations of motion to generate the initial conditions. When using this approach one is restricted to finding periodic orbits that are close to the frozen orbits discussed previously. This is reasonable as one would expect that many periodic orbits would share some of the general properties of the frozen orbits. Since the frozen orbits can be specified analytically in terms of averaged orbital elements it is only necessary to specify that the body-fixed position close in on itself, as then the velocity will similarly close in on itself. In the following only circular orbits are investigated.

To transform an orbit expressed in inertial space (Eq. (36)) into the body-fixed space, pre-multiply the orbit position vector with the transformation matrix Eq. (18) to find the body-fixed position vector:

$$\mathbf{r}_B = r [\cos u(T \cdot \mathbf{r}_\Omega) + \sin u(T \cdot \mathbf{r}_T)] \quad (74)$$

$$(T \cdot \mathbf{r}_\Omega) = \begin{bmatrix} \cos \delta \cos \lambda \\ -\cos(W) \sin \delta \cos \lambda - \sin(W) \sin \lambda \\ \sin(W) \sin \delta \cos \lambda - \cos(W) \sin \lambda \end{bmatrix} \quad (75)$$

$$(T \cdot r_T) = \begin{bmatrix} -\cos i \cos \delta \sin \lambda + \sin \delta \sin i \\ \cos i \cos(W) \sin \delta \sin \lambda - \cos i \sin(W) \cos \lambda + \sin i \cos(W) \cos \delta \\ -\cos i \sin(W) \sin \delta \sin \lambda - \cos i \cos(W) \cos \lambda - \sin i \sin(W) \cos \delta \end{bmatrix} \quad (76)$$

Evaluating the orbit at a partially frozen, circular orbit ($r = a, \lambda = \pm\pi/2$) yields the simplified system:

$$r_B = \mp a \begin{bmatrix} \sin u \cos(\delta \pm i) \\ \cos u \sin(W) - \sin u \cos(W) \sin(\delta \pm i) \\ \cos u \cos(W) + \sin u \sin(W) \sin(\delta \pm i) \end{bmatrix} \quad (77)$$

Sufficient conditions for the orbit to close on itself are then easily noted. First, the angle W must repeat. The period of W is equal to the period of the rotational velocity vector, T . Thus we immediately have the condition that the period of the orbit must be of the form NT . Next, the orbit elements must be chosen so that the period of u is commensurate with NT . The period of u depends on both the true anomaly and the argument of periapsis. Specify the mean frequency of u by n_u , then the period associated with u is $T_u = 2\pi/n_u$. The frequency n_u is computed as:

$$n_u = n + \dot{M}_o + \dot{\omega} \quad (78)$$

Evaluating this at a frozen orbit yields an analytic expression:

$$n_u = n \mp \frac{\sin i \dot{\alpha}}{\sin 2(\delta \pm i)} [2 - 6 \sin^2(\delta \pm i) \pm \cot i \sin 2(\delta \pm i)] \quad (79)$$

where n is the mean motion and the semi-major axis value is chosen according to the frozen orbit rules, so n_u is a function of the assumed value of the relative node ($\pm\pi/2$) and of the inclination. The periodicity condition is then:

$$n_u NT = 2\pi M \quad (80)$$

and the inclination is chosen so that this condition is satisfied for different values of M and N . Figure 11 shows a plot of $n_u T / (2\pi)$ as a function of inclination and Figure 12 shows the same quantity as a function of semi-major axis for circular partially frozen orbits. Note that the positive relative node

frozen orbit solutions only yield periodic orbits with a high commensurability. Given the already unstable nature of orbits in this regime it is doubtful that this approach can yield useful initial conditions for periodic orbits. The orbits with lower commensurability, which should be the easiest to compute numerically, only occur at inclinations close to 0 or 180°. As the inclinations move away from these values the dynamic environment becomes stronger and the sensitivity to initial conditions grows, meaning again that it becomes more difficult to compute orbits given these coarse initial conditions.

Figure 11: The ratio of orbit period frequency with the Toutatis period frequency as a function of inclination along the family of partially frozen orbits. The direct and retrograde negative node and the positive node solutions are shown. Wherever the value of this ratio is a rational number there is potentially a periodic orbit existing in the full equations of motion.

Figure 12: The ratio of orbit period frequency with the Toutatis period frequency as a function of semi-major axis along the family of (circular) partially frozen orbits. The direct and retrograde negative node and the positive node solutions are shown. Wherever the value of this ratio is a rational number there is potentially a periodic orbit existing in the full equations of motion.

These initial conditions have been used successfully to compute the direct and retrograde 1:1 periodic orbits and the 1:2 and 1:3 retrograde periodic orbits, where $N = 1$ is the number of Toutatis periods per $M (= 1, 2, 3)$ particle orbits about Toutatis. The actual transition from the frozen orbit initial conditions to the periodic orbit in the full problem is non-trivial. In only very few cases did the estimated initial conditions yield the proper result. Where this did not work a strategy of estimating the periodic orbit in the presence of the 2nd order gravity field alone worked in many

cases. Once this solution was found, then the order of the gravity field was incrementally increased until the periodic orbit was found in the full degree and order 20 field.

We have computed the complete set of four direct and four retrograde 1:1 periodic orbits. The 1:1 direct orbits have semi-major axes at ~ 13.3 km, eccentricity less than 0.011, and inclination at $\sim 0.4^\circ$. The retrograde 1:1 orbits have semi-major axes at ~ 47.3 km, eccentricity less than 0.00014, and inclination at $\sim 179.995^\circ$. Analysis of these orbits families shows that two of the orbits are stable and two are unstable. The different orbits in each family differ by $\sim 90^\circ$ in argument of periapsis. The unstable orbits have two 1-dimensional hyperbolic manifolds arriving and departing from them. Motion along these unstable manifolds tends to keep the semi-major axis of the orbit conserved and yields bounded oscillations of the eccentricity. This is expected as these orbits lie close to the class of persistent frozen orbits.

The retrograde families at 1:2 and 1:3 were more difficult to compute. The 1:2 orbits have semi-major axes ~ 16.5 km, eccentricity bounded by 0.02 and inclinations at $\sim 179.8^\circ$. The 1:3 orbits have semi-major axes ~ 11.2 km, eccentricity bounded by 0.006 and inclinations at $\sim 179.2^\circ$. All members that have been computed in the full gravity field are found to be stable. Computation of these orbits under the 2nd degree and order gravity field alone is fairly simple. However, extension of those orbits to the full gravity field (or even the 4th degree and order gravity field) are much more difficult. This implies that the large C_{30} gravity term may destroy various family members or cause them to bifurcate into multiple orbits causing our numerical iteration procedure to become less robust (as there may be multiple solutions close to each other in phase space).

Figure 13 shows some of these periodic orbits in the Toutatis body-fixed space. Figure 14 shows three-dimensional renderings of these periodic orbits in the Toutatis body-fixed space.

4.5 Implications of the Rotational State on the Gravity Field

Orbital dynamics about Toutatis would be significantly different were Toutatis in a different rotation state: One can consider the “generic” rotation state of an asteroid to be uniform rotation about its

Figure 13: Periodic orbits about Toutatis shown in three orthographic projections. Shown are: a) All 1:1 Direct periodic orbits, b) One 1:1 Retrograde periodic orbit, c) Two 1:2 Retrograde periodic orbits, d) One 1:3 Retrograde periodic orbit. Integrated using the full equations of motion with no approximation.

Figure 14: Periodic orbits about Toutatis shown rendered in color. Shown are: a) All 1:1 Direct periodic orbits, b) One 1:1 Retrograde periodic orbit, c) One 1:2 Retrograde periodic orbits, d) One 1:3 Retrograde periodic orbit. Integrated using the full equations of motion with no approximation.

maximum moment of inertia, as this is the lowest energy rotation state that a body can have given a fixed value of angular momentum and, assuming dissipation acting over a sufficiently long time span, it is the expected final state of all complex rotators. Were Toutatis in such a configuration, its gravity field expanded about its rotational pole would show a significant change in terms to: $C_{20} = -0.438$, $C_{22} = 0.186$ and $C_{30} = 0.038$, yielding a change in sign and value of C_{20} , an order of magnitude increase in C_{22} and an order of magnitude decrease in C_{30} . Needless to say, the orbital behavior about Toutatis would be significantly different. The main effect of the Toutatis rotation state as compared to the generic case is three-fold: the inclination has large periodic variations, orbits have nominally constant values of energy due to the decreased C_{22} term, and the large C_{30} term induces an oscillation in the eccentricity that can cause impact on the surface of Toutatis. Were Toutatis in the generic rotation state it would have small changes in inclination and larger changes in a and e due to the larger C_{22} term. It would also have smaller changes in e due to the C_{30} term.

5 Dynamics of Surface Particles

5.1 Surface Forces

The force on a particle on Toutatis is the sum of contributions from the asteroid's gravity, the asteroid's rotation, and forces arising from the particle's contact with other particles/surfaces. If the particle is stationary on the surface, then all these forces sum to zero. If the forces are mismatched then the particle will migrate across the Toutatis surface till it finds a configuration where these forces again sum to zero.

The sum of gravitational and rotational accelerations acting on a particle at a position \mathbf{r}_o can be expressed as the vector:

$$V_r(\mathbf{r}_o) = U_r(\mathbf{r}_o) - 2\Omega \times \dot{\mathbf{r}}_o - \Omega \times (\Omega \times \mathbf{r}_o) - \dot{\Omega} \times \mathbf{r}_o \quad (81)$$

The surface contact force acting on the particle is then:

$$N(\mathbf{r}_o) = -V_r(\mathbf{r}_o) \quad (82)$$

if the particle is stationary. In the body-fixed frame the gravitational accelerations are always constant, but the rotational accelerations are time periodic with a period of 5.42 days. Thus, the contact force acting on the particle must also be time-periodic if the particle remains fixed in the Toutatis frame. Were the particle free to roll, like a marble trapped in a depression, we would observe an oscillation of the particle's position with a period of 5.42 days.

Since the rotation rate is so slow, the total variation of this acceleration is small. Were the rotation rate faster the asteroid would shed kinetic energy via such oscillations and relax to principal axis rotation. For Toutatis, Harris (1994) has argued that the time scale for relaxation is longer than the age of the solar system.

To investigate the geography of regolith migration and accumulation, we calculate the normal and tangential components of the force as functions of location. The normal component is found by taking the dot product of the surface force $N(\mathbf{r}, t)$ with the local normal, denoted by the vector

$\mathbf{n}(\mathbf{r})$. Let us suppress the dependence on location:

$$N_n = \mathbf{N} \cdot \mathbf{n} \quad (83)$$

The remaining surface force is then tangent to the local Toutatis surface:

$$\mathbf{N}_t = \mathbf{N} - N_n \mathbf{n} \quad (84)$$

The local slope:

$$\phi = \tan^{-1} |\mathbf{N}_t|/N_n \quad (85)$$

quantifies the degree from which the surface departs that of the geoid. Figure 15 shows this slope computed over the surface of Toutatis. \mathbf{N}_t points toward decreasing ϕ and particles will move in this direction, normal to the constant ϕ (slope) contours. Per our previous discussion, the slope as defined here will vary with time. Figure 16 plots the variation in the slope at several points on the Toutatis surface, note that this variation is rather small. Also note that the slope over the majority of the Toutatis surface is less than 35° , in many places much less than this. This is somewhat surprising given the elongated and rough surface of Toutatis and may be due to the continued shaking that particles on the surface experience.

Figure 15: Slopes over the surface of Toutatis, shown rendered in four perspective views. The viewing geometry is the same as in Figure 2. The slopes range from 0 up to 40° . The higher slopes are at the long ends of the asteroid while the smaller slopes are along the asteroid's waist. The average slope is 16° and 96% of the surface has a slope less than 35° .

The magnitude of the tangential accelerations over the Toutatis surface is of interest as if the total magnitude of the tangent force is small, the local surface forces may easily overwhelm it, allowing for high slopes without the particle slipping. On Toutatis the maximum tangential acceleration is 0.48 mm/s^2 at latitude -10 and longitude -135 degrees, the average value is 0.2

Figure 16: Variation in slope at points on Toutatis. Note that the total variation is small due to the small rotational acceleration of Toutatis. The period of the variation is fixed at 5.42 days, or 130.2 hours.

mm/s², and is less than 0.25 mm/s² over 70% of the surface. The magnitude of the tangential acceleration is highly correlated with the surface slope over Toutatis.

5.2 Surface Escape Speed

The speed needed for a particle to escape Toutatis approximately equals the landing speed of a particle (or spacecraft) approaching from a high orbit. For a non-rotating, spherical body, the escape speed from the surface of that body is independent of the direction of the initial velocity (if the trajectory does not re-intersect the body). For bodies with rotation the direction of the initial velocity will change the escape speed of the particle. For example, if the initial velocity points in the same sense as the body rotation direction, the escape speed will be lowered. If the body has a non-spherical shape there is a further complication to the computation of escape speed, because the true escape speed of a particle launched from the surface will also depend on the gravity field that it interacts with after launch.

Let us compute the escape speed considering only the local gravity, the total mass of the body, and the rotational motion of the body. We assume that a particle leaves the asteroid normal to the local surface: $\mathbf{v} = v\mathbf{n}$ where \mathbf{n} is the local normal to the surface and v is the launch speed. Then the particle's inertial velocity is:

$$\mathbf{v}_I = v\mathbf{n} + \boldsymbol{\Omega} \times \mathbf{r} \quad (86)$$

where \mathbf{r} is the vector to the surface and $\boldsymbol{\Omega}$ is the asteroid's angular velocity vector. To find the local escape speed, set the magnitude of the inertial velocity equal to $\sqrt{2U_{\max}(\mathbf{r})}$ where $U_{\max}(\mathbf{r}) =$

$\max(U(\mathbf{r}), \mu/|\mathbf{r}|)$. Evaluating this condition and solving the resulting quadratic equation yields:

$$v(\mathbf{r}) = -\mathbf{n} \cdot (\boldsymbol{\Omega} \times \mathbf{r}) + \sqrt{[\mathbf{n} \cdot (\boldsymbol{\Omega} \times \mathbf{r})]^2 + 2U_{\max}(\mathbf{r}) - (\boldsymbol{\Omega} \times \mathbf{r})^2} \quad (87)$$

This quantity has been computed over the surface of Toutatis using the polyhedral gravitational field (Figure 17) and is between 1.2 and 1.8 m/s over most of the surface. The escape speeds also have a periodic variation which is, again, small. Comparisons between these computed escape speeds and numerical integrations of particles leaving the surface with the same velocity show good agreement in that the numerically integrated particles in general escape from Toutatis. Thus, these numbers are reasonable maximum bounds on ejecta speeds which do not escape from Toutatis.

Figure 17: Local normal escape speed over the Toutatis surface, shown rendered in four perspective views. The viewing geometry is the same as in Figure 2. The contribution of the angular velocity to the escape speed is small, hence the variation in these speeds are due mostly to the gravitational field of Toutatis.

Figure 18: Change in local normal escape speed at points on Toutatis. The total variation of the escape speeds is less than a few centimeters per second, much less than this over most of the body. The period of this variation is 5.42 days or 130.2 hours.

5.3 Dynamics of Ejected Particles

What is the final evolution of a particle launched from Toutatis with less than escape speed? The short answer is that it will re-impact the asteroid. Though this sounds like an obvious answer, it is not necessarily true for uniformly rotating asteroids. In those situations the effect of the C_{22} term of the gravity field is to change the semi-major axis (or energy) of the orbit significantly over one orbit

of the body, allowing a particle with an initial sub-escape speed to gain escape speed and leave the body (Scheeres et al 1996). Toutatis' C_{22} gravity term is small enough and its rotational motion not of the proper form so that that these post-launch energy effects are very small and do not contribute to more ejecta leaving the system. The time scale for a particle to re-impact on Toutatis can be quite long, however.

There are several factors contributing to the potential longevity of ejected particles remaining in orbit: the complex motion of Toutatis, the persistence of the frozen orbits in the real Toutatis system and the lack of large variations in orbit energy due to a small C_{22} term. The complex motion of Toutatis in inertial space allows a particle to avoid re-impacting at its first return to periapsis. Whereas the original orbit's periapsis would lie beneath the Toutatis surface by definition, since the asteroid moves in inertial space it is possible that at the next periapsis passage that the asteroid will no longer be in the proper place and time for impact to occur. In a dynamical environment such as Toutatis' this is sufficient time for the orbit to change into a form that avoids impact for a sustained period of time. Of course, only a sub-set of the total number of particles ejected randomly will avoid immediate impact.

It is after the ejected particle fails to impact within the first few orbits that the persistence of the frozen orbits play a factor. As discussed earlier, the persistence of the frozen orbits close to Toutatis does not imply that they are stable orbits. One expects these orbits (more precisely these regions of phase space) to be ultimately unstable, instability in this case meaning that the particles will re-impact the Toutatis surface at some future time. The instability associated with these orbits is hyperbolic with some of them having a very long time constant. Then, as this is a Hamiltonian system, the existence of the unstable manifolds also implies the existence of similarly slow stable manifolds, leaving open the possibility that a particle could become entrained in the stable manifold of a frozen orbit region of the phase space and approach the region closely before departing on an unstable manifold leading to an impact. As examples we have found orbits which leave the Toutatis surface, hang out in the vicinity of a frozen orbit and then re-impact onto Toutatis, the entire orbit

lasting for a few hundred days. Figure 19 shows the eccentricity, semi-major axis and periapsis radius of such an orbit lasting ~ 257 days from ejection to impact. Figure 20 shows three different re-impacting ejecta orbits with hang-times of different lengths, these views are taken from DeJong et al., 1997.

Figure 19: Re-impacting ejecta over 257 days. Shown are: a) Eccentricity, b) Semi-Major Axis c) Periapsis radius. Integrated using the full equations of motion with no approximation.

Figure 20: Re-impacting ejecta orbits at Toutatis shown in body-fixed (lhs) and inertial (rhs) coordinate frames. Shown are: a) Orbit duration of 1.24 days, b) Orbit duration of 2.93 days, c) Orbit duration of 167.94 days.

Since Toutatis does not impose large energy variations on an orbiting particle, the lifetime of an orbit is significantly extended as compared to the environment of a uniformly rotating asteroid. The practical upshot of this is that after a meteorite impacts Toutatis, ejecta may persist in orbit for extended periods of time.

5.4 Distribution of Returning Ejecta

How will returning ejecta be distributed over the surface of Toutatis? This is a difficult question best addressed, perhaps, by simulating impacts and tracking the evolution of the ejecta that do not escape, considering secondary and perhaps higher generation impacts. We have not done such simulations for Toutatis, but some inferences about ejecta distribution are possible now. In terms of geometric cross-section, it is clear that the ends of Toutatis will be more difficult to hit and that the long, slender regions of Toutatis will be easier to hit. Since the rotational velocity of Toutatis is small, ejecta are not expected to fall preferentially on the leading edge of the asteroid. Rather, due

to Toutatis' complex rotation state one would expect the infall of ejected particles to be distributed more uniformly across the surface of the body for the following reasons.

First, the complex rotation of the body will present any given patch of its surface to a larger range of angular orientations in the sky over time than if it were in uniform rotation. Thus, depending on when a given particle falls back onto the surface, there is a larger pool of potential impact locations. Moreover, as described above, the inclination of a particle's orbit can have large changes in a fairly short time span. Changes in orbital inclination correspond to the particle's angular position about the asteroid being distributed over a larger range than with a uniform rotator. This again would lead to larger range of surface locations on which the re-impacting particle may fall. These effects are in contrast to simulations of the distribution of ejecta on the surface of a uniformly rotating asteroid (Scheeres et al., 1996), which show a preference for ejecta accumulation on the leading edges and a general migration of re-impacting ejecta towards the asteroid's poles if the effect of a non-zero coefficient of restitution is modeled in the re-impact dynamics.

6 Conclusions

This paper is a first step toward a comprehensive understanding of close-orbit dynamics about a body of arbitrary shape and spin state. The dynamics of orbits close to Toutatis clearly are very different from the dynamics of orbits close to a uniform rotator, and to some degree are a product of this asteroid's unusual shape.

Issues raised in this paper that deserve further attention include the computation of periodic orbits around complex rotators and the refinement of analytic solutions to the averaged equations of motion. This paper also sets the stage for detailed exploration of the dynamics of non-escaping impact ejecta as a function of impact location and energy, with the goal of understanding the geography of regolith redistribution on the asteroid's surface.

Acknowledgments

Part of the research described in this paper was carried out by the Jet Propulsion Laboratory, California Institute of Technology, under contract with the National Aeronautics and Space Administration. RSH acknowledges support by NASA.

References

- Belton, M. J. S., C. R. Chapman, P. C. Thomas, M. E. Davies, R. Greenberg, K. Klaasen, D. Byrnes, L. D'Amario, S. Synnott, T. V. Johnson, A. McEwen, W. J. Merline, D. R. Davis, J-M. Petit, A. Storrs, J. Veverka, and B. Zellner 1995. Bulk density of asteroid 243 Ida from the orbit of its satellite Dactyl. *Nature* **374**, 785-788.
- Brouwer, D., G.M. Clemence, 1961. *Methods of Celestial Mechanics*, Academic Press.
- DeJong, E., S. Suzuki 1997. Visualization of Earth-Approaching Asteroids, JPL video AVC-97-061.
- Hamilton, D.P., J.A. Burns 1991. Orbital stability zones about asteroids, *Icarus*, **92**, 118 - 131.
- Harris, A.W. 1994. Tumbling asteroids, *Icarus*, **107**, 209 - 211.
- Hudson, R.S., S.J. Ostro, 1995. Shape and non-principal axis spin state of asteroid 4179 Toutatis, *Science*, **270**, 84-86.
- Hudson, R.S., S.J. Ostro 1994. Shape of asteroid 4769 Castalia (1989 PB) from inversion of radar images. *Science*, **263**, 940 - 943.
- Kaula, W.M. 1966. *Theory of Satellite Geodesy*, Blaisdell.
- MacMillan, W.D., 1960. *Dynamics of Rigid Bodies*, Dover.
- Ostro, S.J., R. F. Jurgens, K. D. Rosema, R. S. Hudson, J. D. Giorgini, R. Winkler, D.K. Yeomans, D. Choate, R. Rose, M. A. Slade, S. D. Howard, D. J. Scheeres, and D. L. Mitchell 1996. Radar observations of asteroid 1620 Geographos. *Icarus*, **121**, 44-66.
- Ostro, S.J., R.S. Hudson, R.F. Jurgens, K.D. Rosema, D.B. Campbell, D.K. Yeomans, J.F. Chandler, J.D. Giorgini, R. Winkler, R. Rose, S.D. Howard, M.A. Slade, P. Perillat, I.I. Shapiro, 1995. Radar images of asteroid 4179 Toutatis, *Science* **270**, 80 - 83.

- Scheeres, D.J., S.J. Ostro, R.S. Hudson, R.A. Werner, 1996. Orbits close to asteroid 4769 Castalia, *Icarus* **121**, pp 67-87.
- Scheeres, D.J. 1995. Analysis of orbital motion around 433 Eros, *J. Astronautical Sciences*, **43**, 4, pp 427-452.
- Scheeres, D.J. 1994a. Dynamics about uniformly rotating tri-axial ellipsoids, *Icarus*, **110**, 2, pp 225 - 238.
- Scheeres, D.J. 1994b. Satellite dynamics about asteroids, in *Spaceflight Mechanics 1994, Advances in the Astronautical Sciences Series*, Vol. 87, No. 1, pp 275-292.
- Werner, R.A., D.J. Scheeres, 1997. Exterior gravitation of a polyhedron derived and compared with harmonic and mascon gravitation representations of asteroid 4769 Castalia, *Celestial Mechanics*, **65**, 313-344.
- Werner, R.A. 1994. The gravitational potential of a homogeneous polyhedron, *Celestial Mechanics*, **59**, 253-278.
- Whittaker, E.T., G.N. Watson 1952. *Modern Analysis*, 4th Ed., Cambridge.

Orbit dynamics about 4179 Toutatis

D.J. Scheeres, S.J. Ostro, R.S. Hudson, E.M. DeJong, S. Suzuki

Figure 1: Radius contours of Toutatis.

Figure 2: The shape of Toutatis and its coordinate axes shown rendered in four perspective views.

Figure 3: Number of Toutatis revolutions per particle orbit. Three regimes are identified here, the sub-resonant regime where the particle has multiple orbits per Toutatis rotation, the resonant regime where the orbit and Toutatis period are approximately equal, and the super-resonant regime where Toutatis has multiple rotations per particle orbit.

Figure 4: Semi-major axis for a frozen circular orbit as a function of inclination and node λ . Derived using the averaged equations with C_{20} only.

Figure 5: The evolution of the inclination and relative node for different initial values of the node λ for orbits with initial values $a = 3.0, e = 0, i = 70$, which are frozen initial conditions for $\lambda = \pi/2$. Here, $\lambda = \pi/2$ yields the frozen solution while $\lambda = -\pi/2$ yields the maximum excursion in the inclination. Integrated using the averaged equations with C_{20} only.

Figure 6: The evolution of the inclination and relative node for different initial values of the node λ for orbits with initial values $a = 3.3, e = 0, i = 27$, which are frozen initial conditions for $\lambda = -\pi/2$. Here, $\lambda = -\pi/2$ yields the frozen solution while $\lambda = \pi/2$ yields the maximum excursion in the inclination. Integrated using the averaged equations with C_{20} only.

Figure 7: The evolution of the averaged inclination over 100 days starting in a frozen orbit (including a frozen argument of periapsis) with $\omega = \pm 90$. The $\omega = \pi/2$ case has a stable eccentricity variation while the $\omega = -\pi/2$ case is unstable. Integrated using the averaged equations with both C_{20} and C_{30} .

Figure 8: The evolution of the averaged periapsis radius over 100 days starting in a frozen orbit (including a frozen argument of periapsis) with $\omega = \pm 90$. The $\omega = \pi/2$ case has a stable eccentricity variation while the $\omega = -\pi/2$ case is unstable. Integrated using the averaged equations with both C_{20} and C_{30} .

Figure 9: Semi-major axis and eccentricity relations for the direct and retrograde fully frozen orbits. The corresponding radius of periapsis is also shown. Derived using the averaged equations with both C_{20} and C_{30} .

Figure 10: Frozen orbit plotted in the Toutatis-fixed frame over 100 days. Initial condition is a circular retrograde frozen orbit with semi-major axis of 3 km, inclination of 139° . Integrated using the full equations of motion with no approximation.

Figure 11: The ratio of orbit period frequency with the Toutatis period frequency as a function of inclination along the family of partially frozen orbits. The direct and retrograde negative node and the positive node solutions are shown. Wherever the value of this ratio is a rational number there is potentially a periodic orbit existing in the full equations of motion.

Figure 12: The ratio of orbit period frequency with the Toutatis period frequency as a function of semi-major axis along the family of (circular) partially frozen orbits. The direct and retrograde

negative node and the positive node solutions are shown. Wherever the value of this ratio is a rational number there is potentially a periodic orbit existing in the full equations of motion.

Figure 13: Periodic orbits about Toutatis shown in three orthographic projections. Shown are: a) All 1:1 Direct periodic orbits, b) One 1:1 Retrograde periodic orbit, c) Two 1:2 Retrograde periodic orbits, d) One 1:3 Retrograde periodic orbit. Integrated using the full equations of motion with no approximation.

Figure 14: Periodic orbits about Toutatis shown rendered in color. Shown are: a) All 1:1 Direct periodic orbits, b) One 1:1 Retrograde periodic orbit, c) One 1:2 Retrograde periodic orbits, d) One 1:3 Retrograde periodic orbit. Integrated using the full equations of motion with no approximation.

Figure 15: Slopes over the surface of Toutatis, shown rendered in four perspective views. The viewing geometry is the same as in Figure 2. The slopes range from 0 up to 40°. The higher slopes are at the long ends of the asteroid while the smaller slopes are along the asteroid's waist. The average slope is 16° and 96% of the surface has a slope less than 35°.

Figure 16: Variation in slope at points on Toutatis. Note that the total variation is small due to the small rotational acceleration of Toutatis. The period of the variation is fixed at 5.42 days, or 130.2 hours.

Figure 17: Local normal escape speed over the Toutatis surface, shown rendered in four perspective views. The viewing geometry is the same as in Figure 2. The contribution of the angular velocity to the escape speed is small, hence the variation in these speeds are due mostly to the gravitational field of Toutatis.

Figure 18: Change in local normal escape speed at points on Toutatis. The total variation of the escape speeds is less than a few centimeters per second, much less than this over most of the body. The period of this variation is 5.42 days or 130.2 hours.

Figure 19: Re-impacting ejecta over 257 days. Shown are: a) Eccentricity, b) Semi-Major Axis c) Periapsis radius. Integrated using the full equations of motion with no approximation.

Figure 20: Re-impacting ejecta orbits at Toutatis shown in body-fixed (lhs) and inertial (rhs) coordinate frames. Shown are: a) Orbit duration of 1.24 days, b) Orbit duration of 2.93 days, c) Orbit duration of 167.94 days.

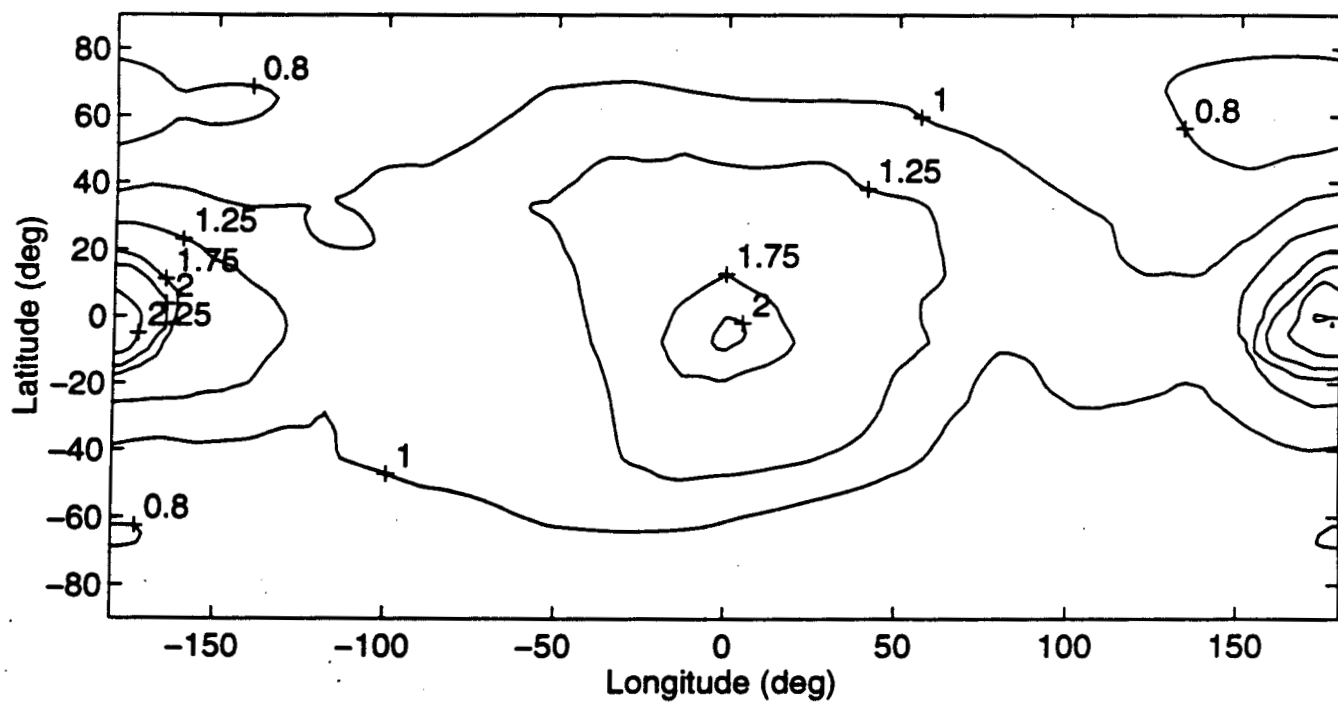


Figure 1: Radius contours of Toutatis.

p-18751

Figure 2: The shape of Toutatis and its coordinate axes shown rendered in four perspective views.

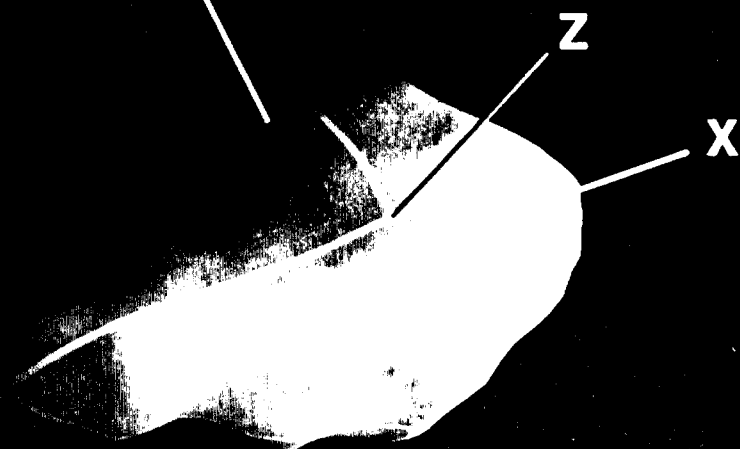
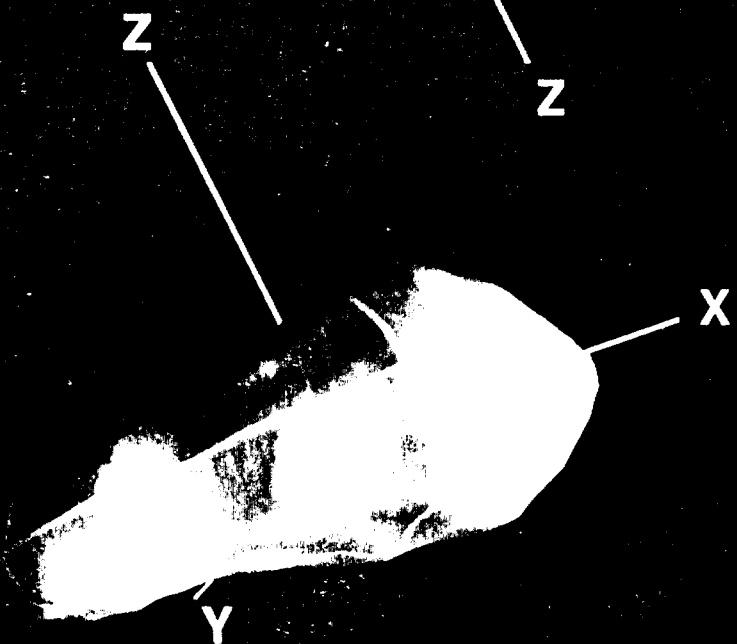
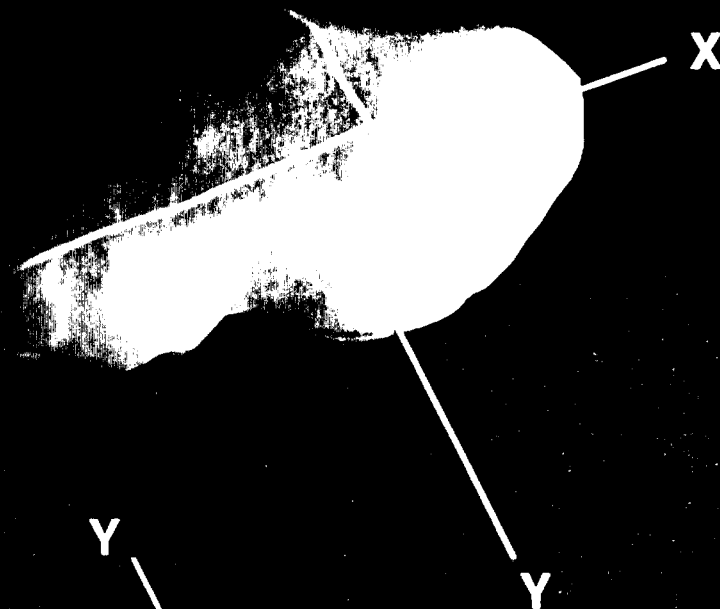
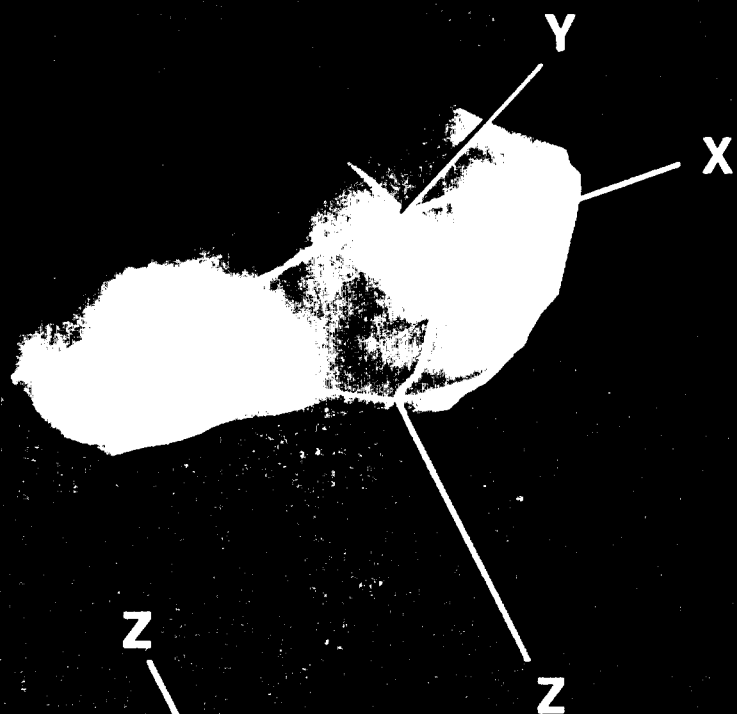


Figure 2

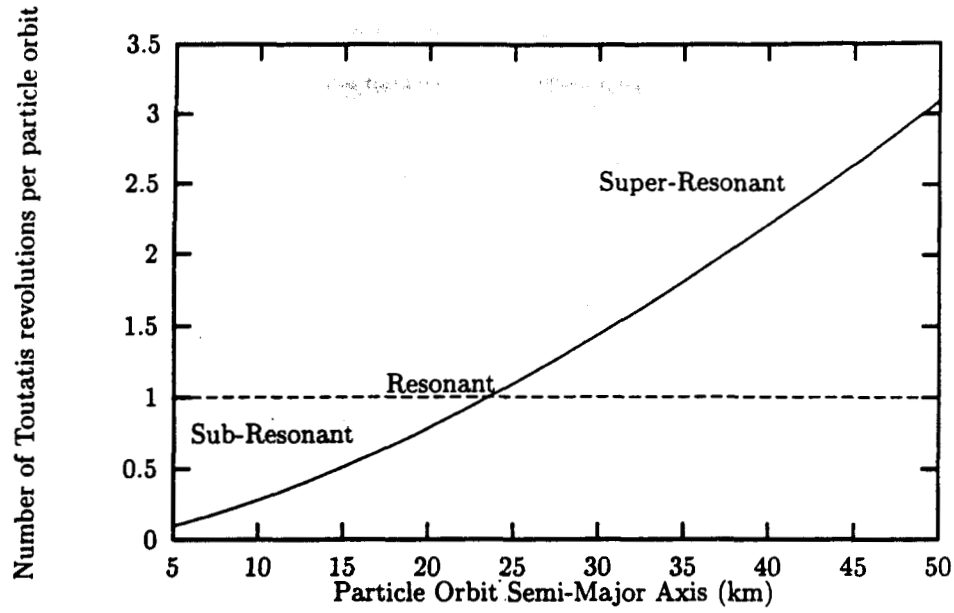


Figure 3: Number of Toutatis revolutions per particle orbit. Three regimes are identified here, the sub-resonant regime where the particle has multiple orbits per Toutatis rotation, the resonant regime where the orbit and Toutatis period are approximately equal, and the super-resonant regime where Toutatis has multiple rotations per particle orbit.

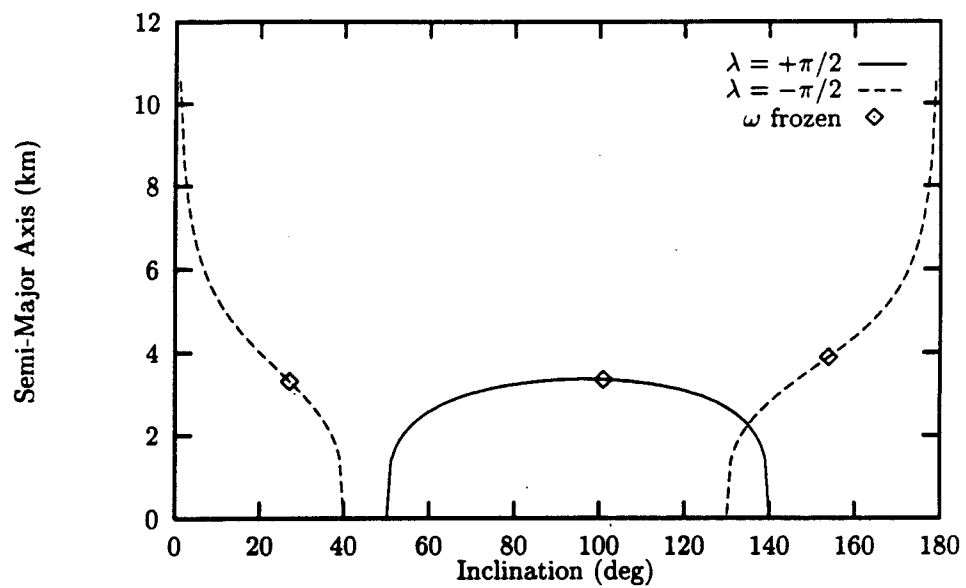


Figure 4: Semi-major axis for a frozen circular orbit as a function of inclination and node λ . Derived using the averaged equations with C_{20} only.

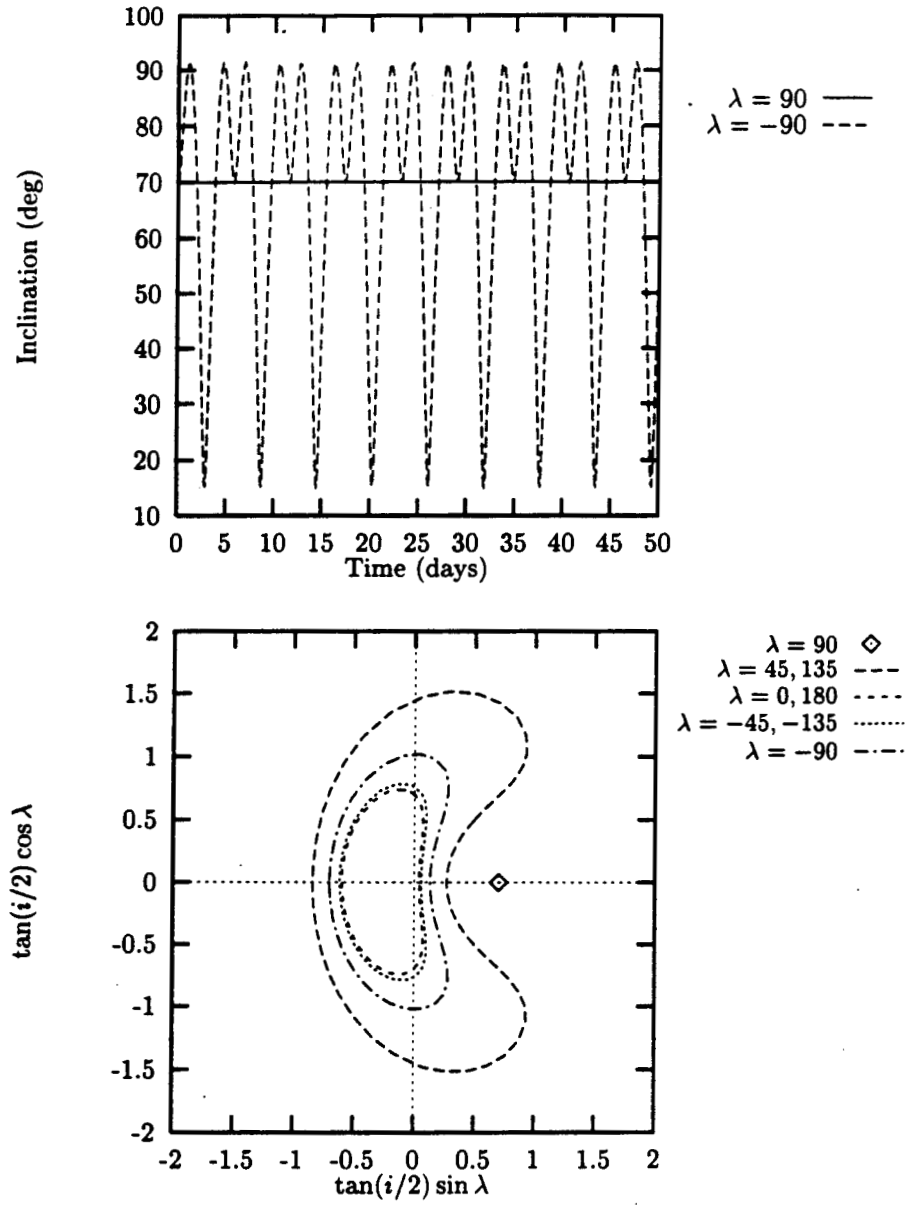


Figure 5: The evolution of the inclination and relative node for different initial values of the node λ for orbits with initial values $a = 3.0, e = 0, i = 70$, which are frozen initial conditions for $\lambda = \pi/2$. Here, $\lambda = \pi/2$ yields the frozen solution while $\lambda = -\pi/2$ yields the maximum excursion in the inclination. Integrated using the averaged equations with C_{20} only.

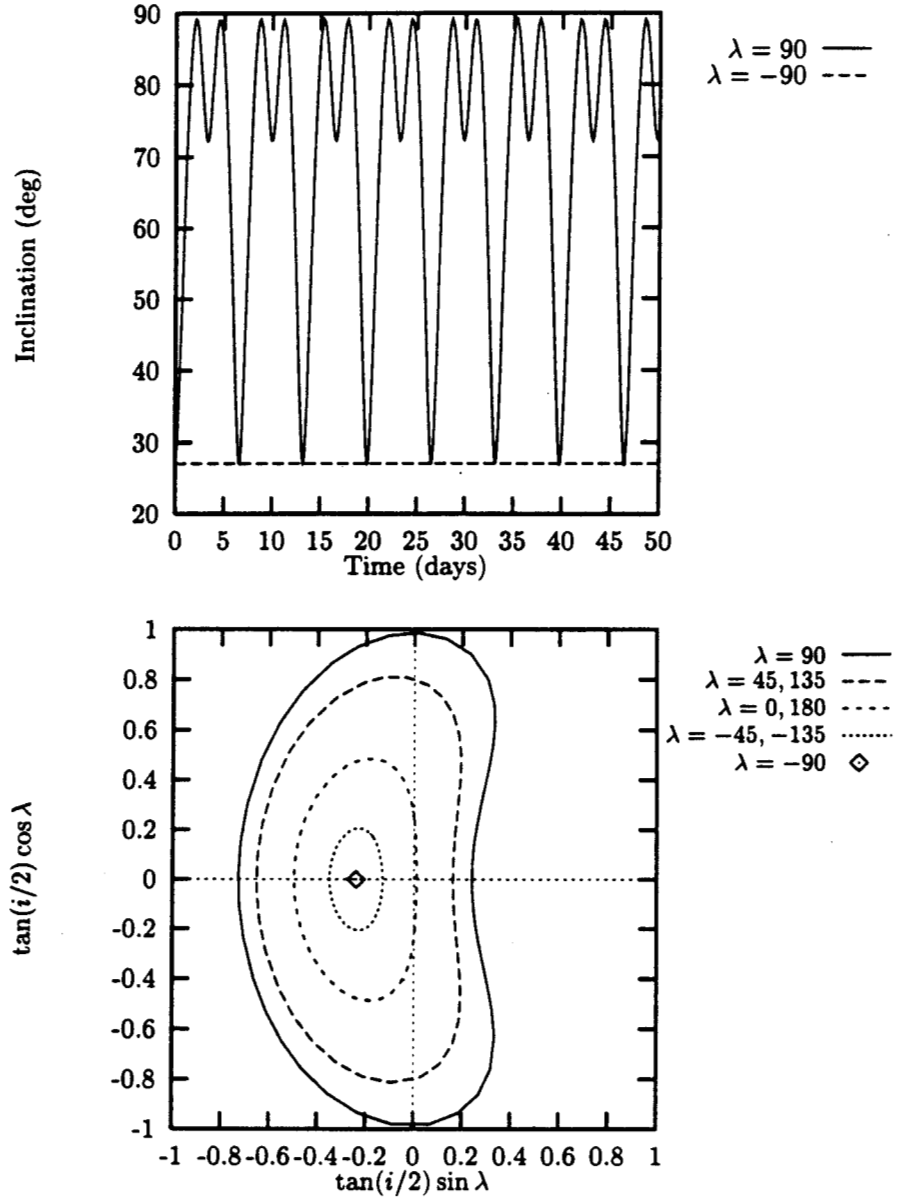


Figure 6: The evolution of the inclination and relative node for different initial values of the node λ for orbits with initial values $a = 3.3, e = 0, i = 27$, which are frozen initial conditions for $\lambda = -\pi/2$. Here, $\lambda = -\pi/2$ yields the frozen solution while $\lambda = \pi/2$ yields the maximum excursion in the inclination. Integrated using the averaged equations with C_{20} only.

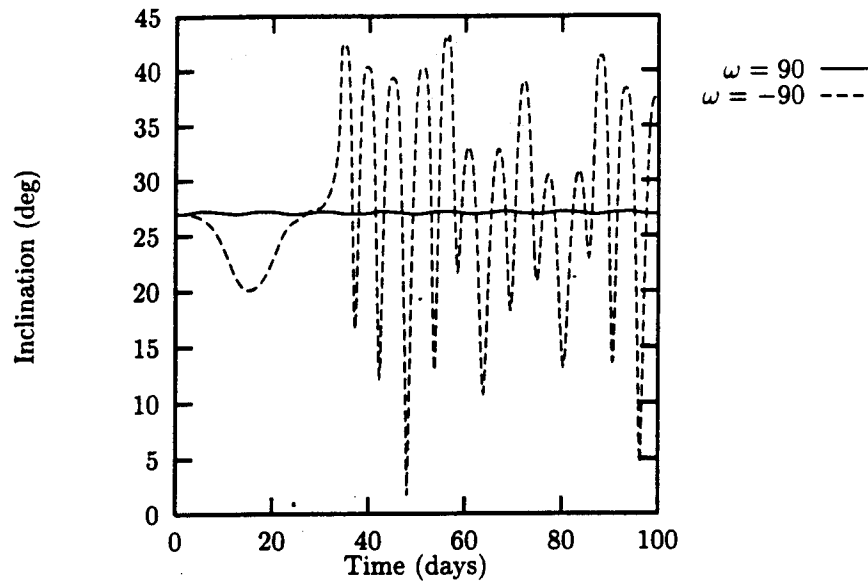


Figure 7: The evolution of the averaged inclination over 100 days starting in a frozen orbit (including a frozen argument of periapsis) with $\omega = \pm 90$. The $\omega = \pi/2$ case has a stable eccentricity variation while the $\omega = -\pi/2$ case is unstable. Integrated using the averaged equations with both C_{20} and C_{30} .

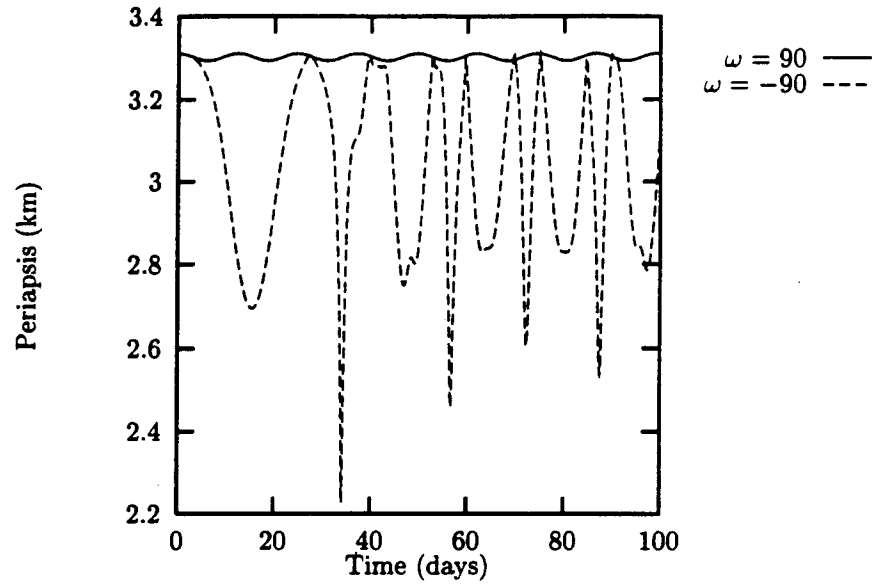


Figure 8: The evolution of the averaged periapsis radius over 100 days starting in a frozen orbit (including a frozen argument of periapsis) with $\omega = \pm 90$. The $\omega = \pi/2$ case has a stable eccentricity variation while the $\omega = -\pi/2$ case is unstable. Integrated using the averaged equations with both C_{20} and C_{30} .

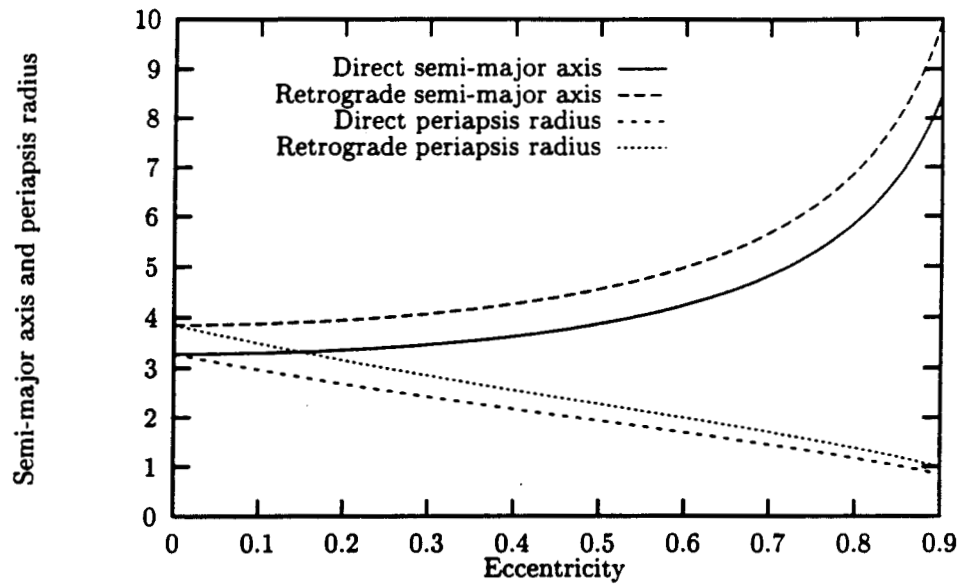


Figure 9: Semi-major axis and eccentricity relations for the direct and retrograde fully frozen orbits. The corresponding radius of periapsis is also shown. Derived using the averaged equations with both C_{20} and C_{30} .

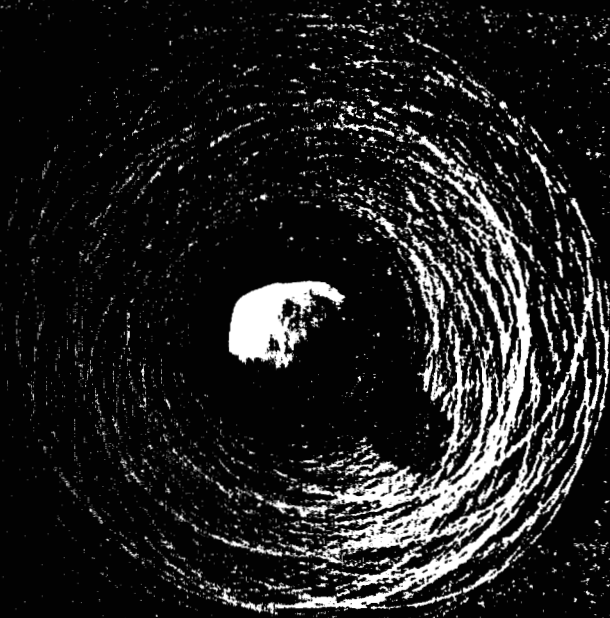


Figure 10

TCP

Figure 10: Frozen orbit plotted in the Toutatis-fixed frame over 100 days. Initial condition is a circular retrograde frozen orbit with semi-major axis of 3 km, inclination of 139° . Integrated using the full equations of motion with no approximation.

P-40700

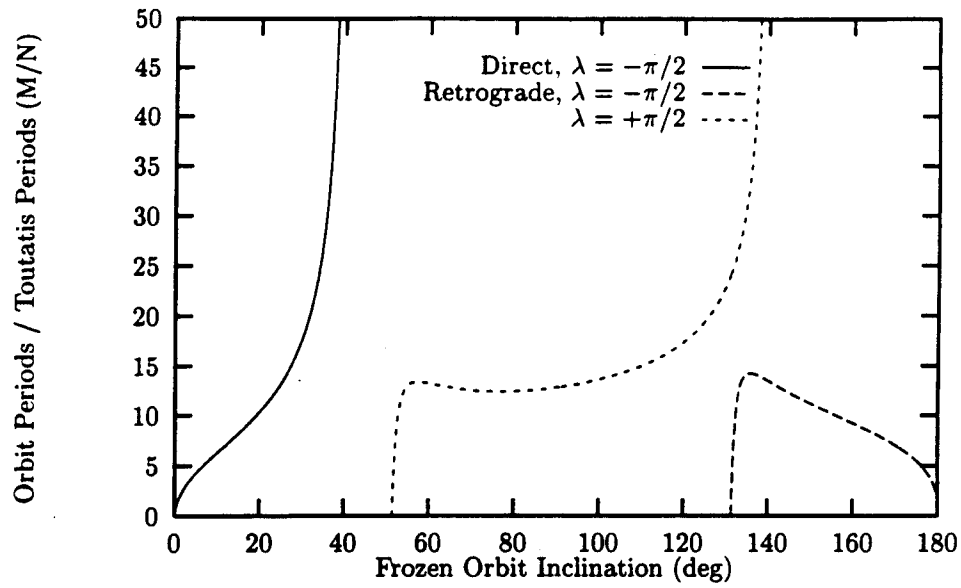


Figure 11: The ratio of orbit period frequency with the Toutatis period frequency as a function of inclination along the family of partially frozen orbits. The direct and retrograde negative node and the positive node solutions are shown. Wherever the value of this ratio is a rational number there is potentially a periodic orbit existing in the full equations of motion.

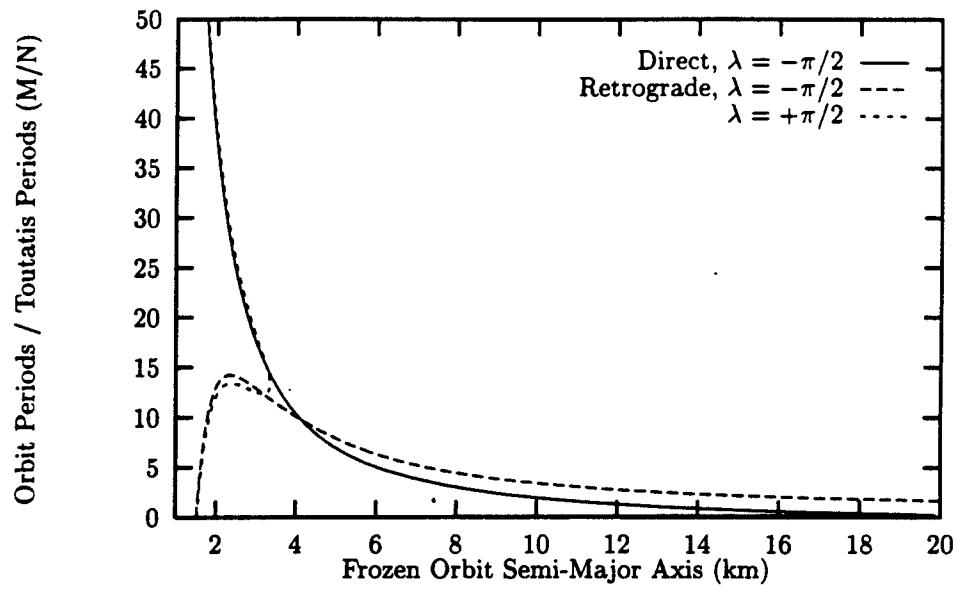
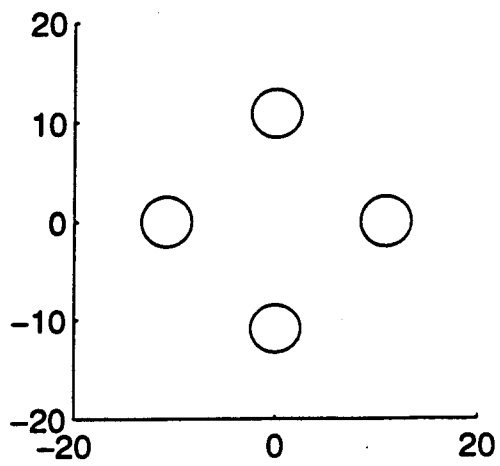
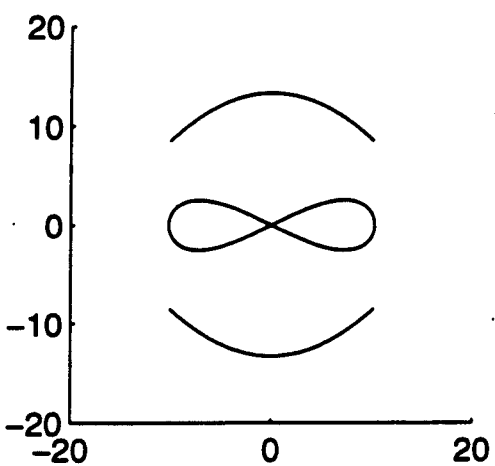
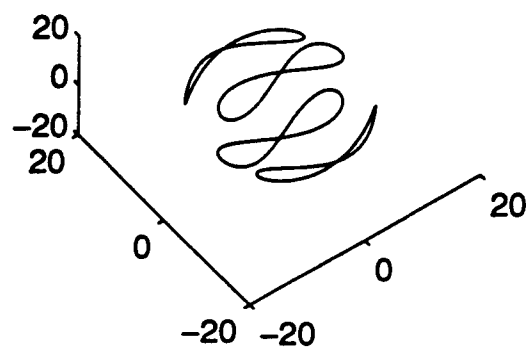
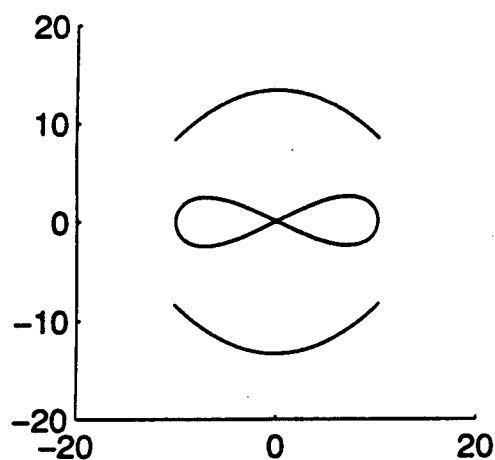
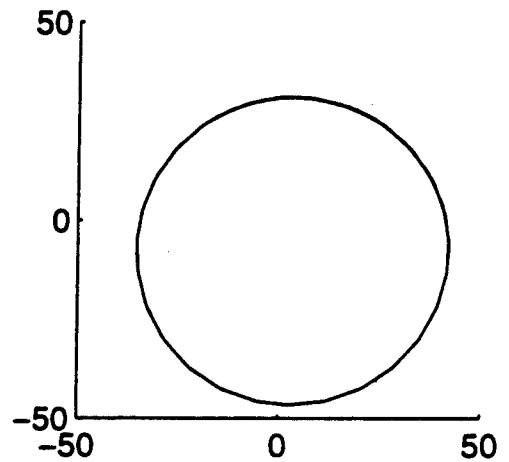
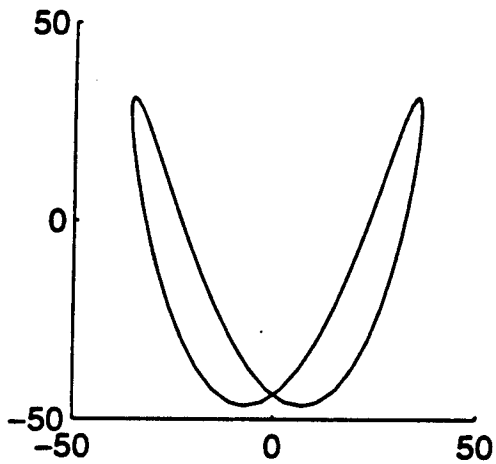
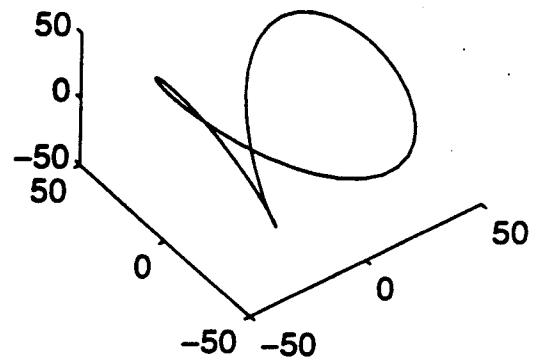
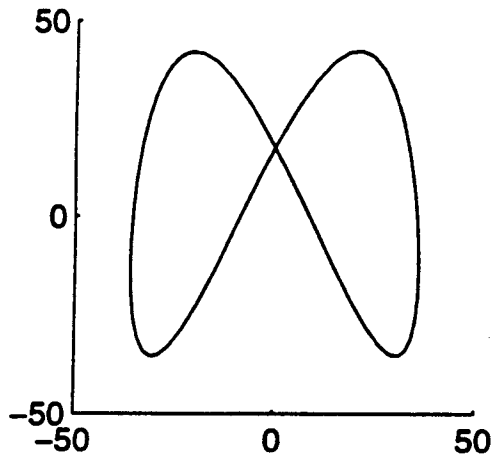


Figure 12: The ratio of orbit period frequency with the Toutatis period frequency as a function of semi-major axis along the family of (circular) partially frozen orbits. The direct and retrograde negative node and the positive node solutions are shown. Wherever the value of this ratio is a rational number there is potentially a periodic orbit existing in the full equations of motion.



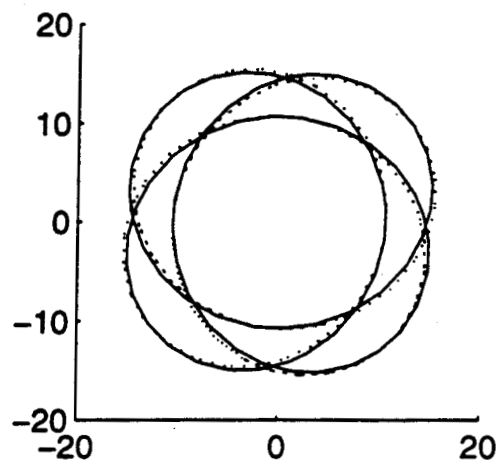
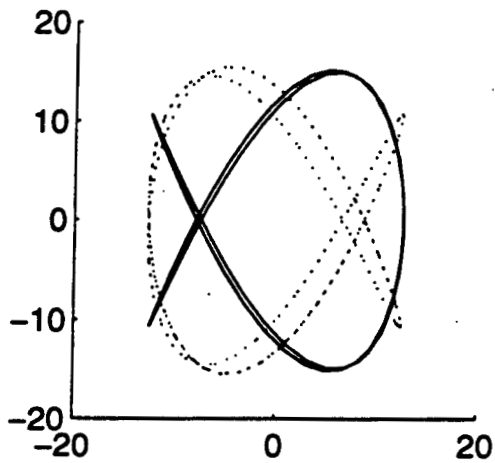
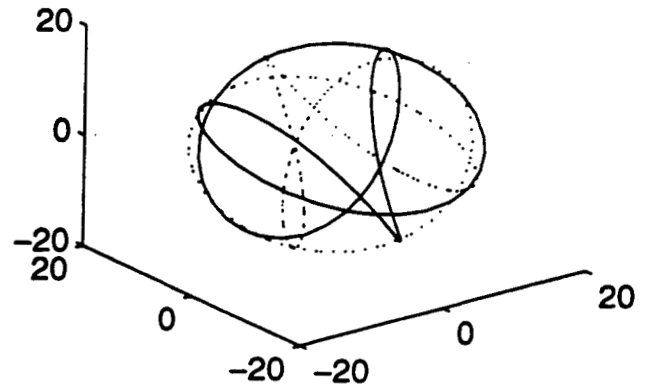
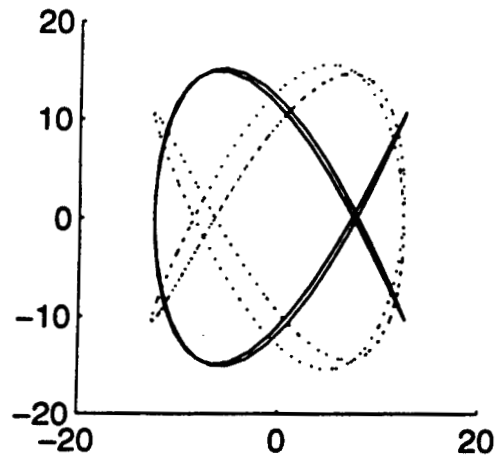
13a

Figure 13: Periodic orbits about Toutatis shown in three orthographic projections. Shown are: a) All 1:1 Direct periodic orbits, b) One 1:1 Retrograde periodic orbit, c) Two 1:2 Retrograde periodic orbits, d) One 1:3 Retrograde periodic orbit. Integrated using the full equations of motion with no approximation.



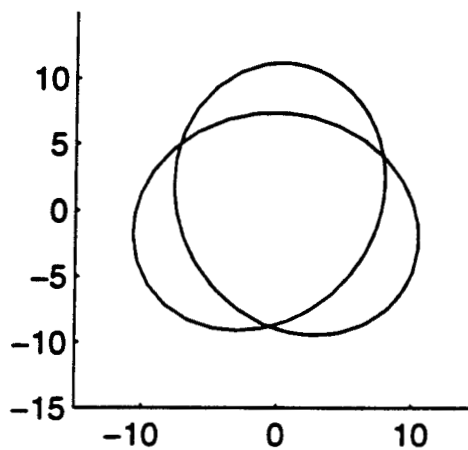
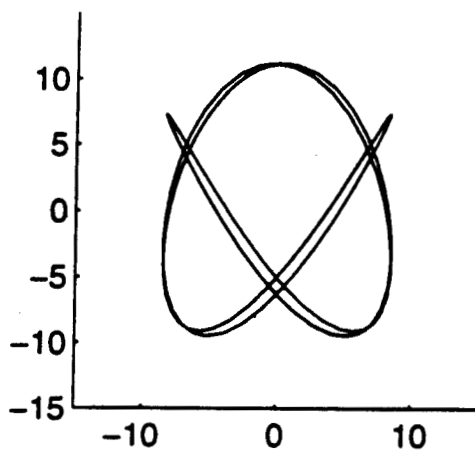
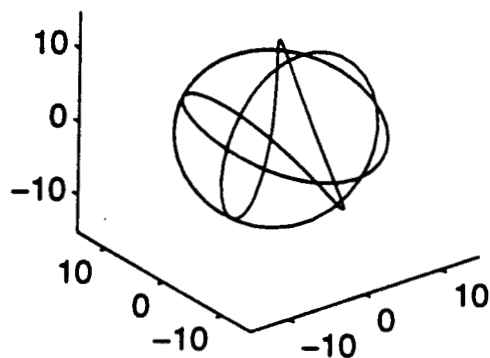
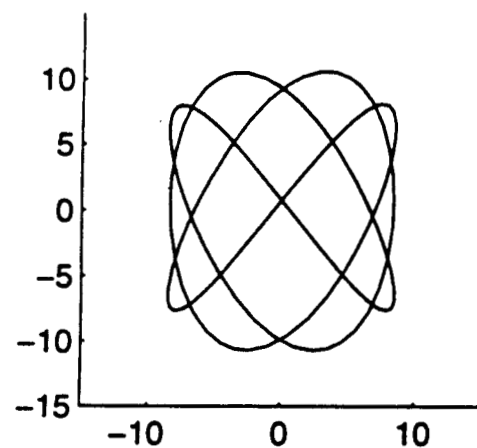
13 b

Figure 13: Periodic orbits about Toutatis shown in three orthographic projections. Shown are: a) All 1:1 Direct periodic orbits, b) One 1:1 Retrograde periodic orbit, c) Two 1:2 Retrograde periodic orbits, d) One 1:3 Retrograde periodic orbit. Integrated using the full equations of motion with no approximation.



13c

Figure 13: Periodic orbits about Toutatis shown in three orthographic projections. Shown are: a) All 1:1 Direct periodic orbits, b) One 1:1 Retrograde periodic orbit, c) Two 1:2 Retrograde periodic orbits, d) One 1:3 Retrograde periodic orbit. Integrated using the full equations of motion with no approximation.



13d

Figure 13: Periodic orbits about Toutatis shown in three orthographic projections. Shown are: a) All 1:1 Direct periodic orbits, b) One 1:1 Retrograde periodic orbit, c) Two 1:2 Retrograde periodic orbits, d) One 1:3 Retrograde periodic orbit. Integrated using the full equations of motion with no approximation.

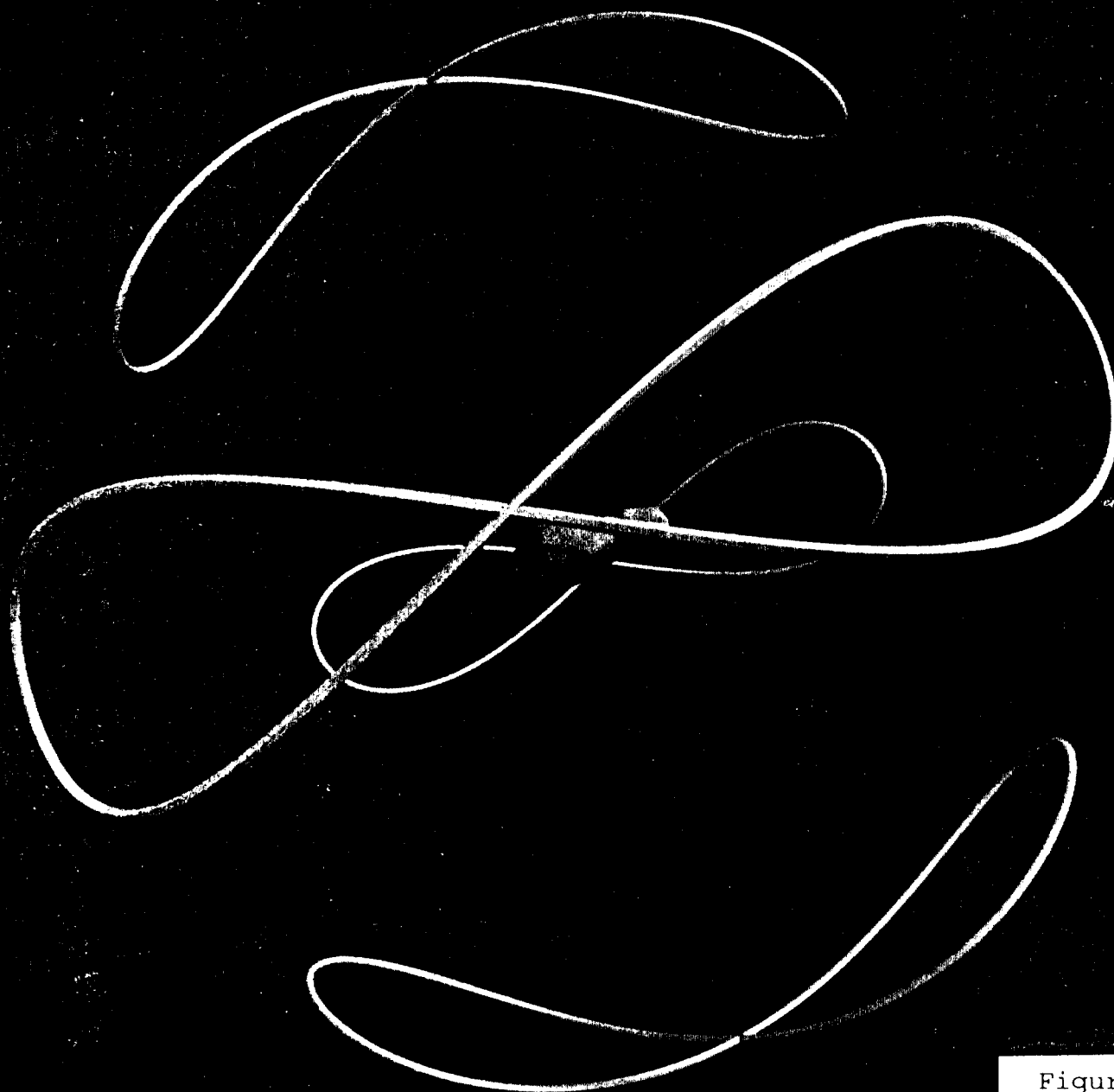


Figure 14a

Figure 14: Periodic orbits about Toutatis shown rendered in color. Shown are: a) All 1:1 Direct periodic orbits, b) One 1:1 Retrograde periodic orbit, c) One 1:2 Retrograde periodic orbits, d) One 1:3 Retrograde periodic orbit. Integrated using the full equations of motion with no approximation.



Figure 14b

Figure 14: Periodic orbits about Toutatis shown rendered in color. Shown are: a) All 1:1 Direct periodic orbits, b) One 1:1 Retrograde periodic orbit, c) One 1:2 Retrograde periodic orbits, d) One 1:3 Retrograde periodic orbit. Integrated using the full equations of motion with no approximation.

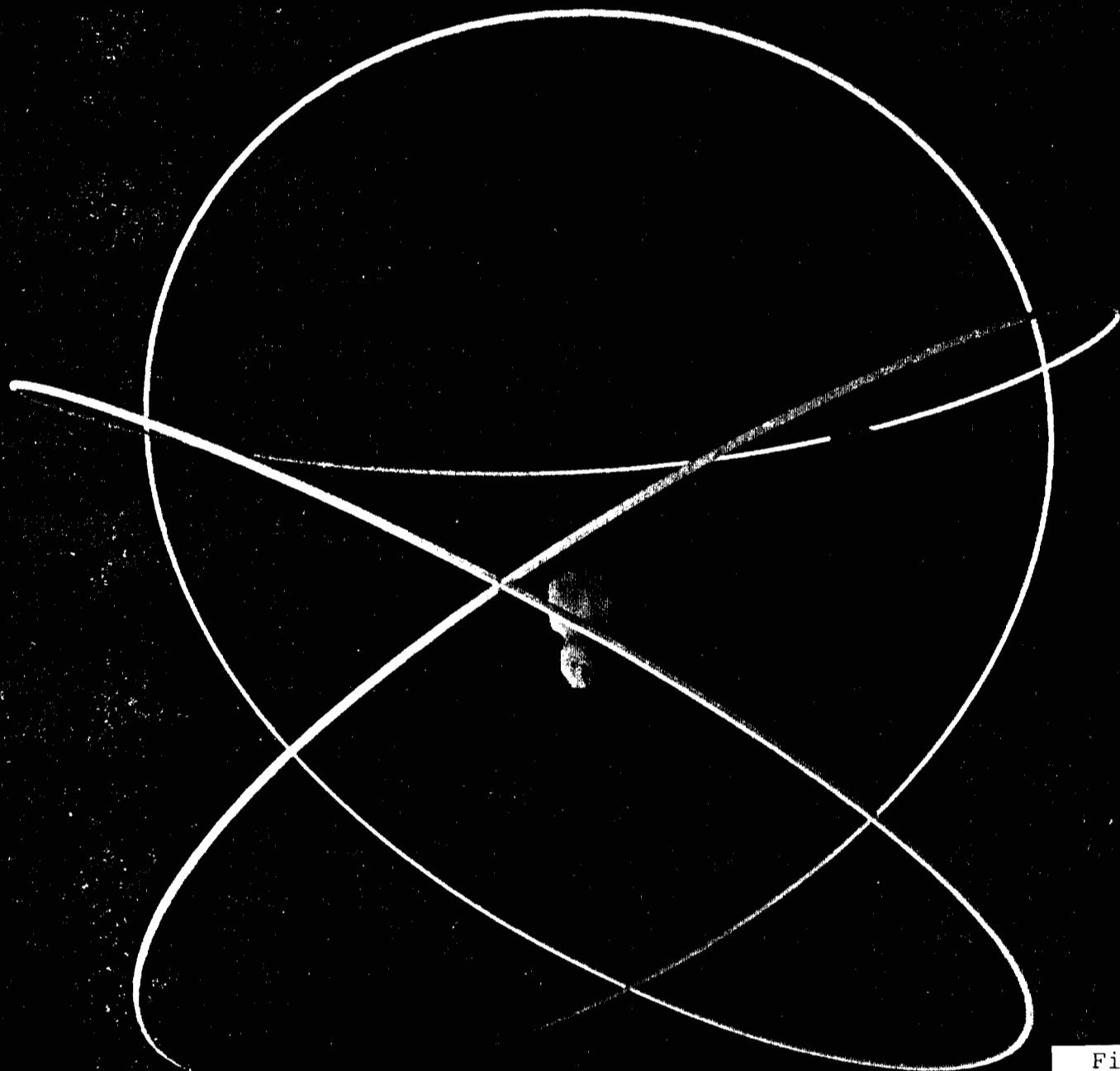


Figure 14c

Figure 14: Periodic orbits about Toutatis shown rendered in color. Shown are: a) All 1:1 Direct periodic orbits, b) One 1:1 Retrograde periodic orbit, c) One 1:2 Retrograde periodic orbits, d) One 1:3 Retrograde periodic orbit. Integrated using the full equations of motion with no approximation.

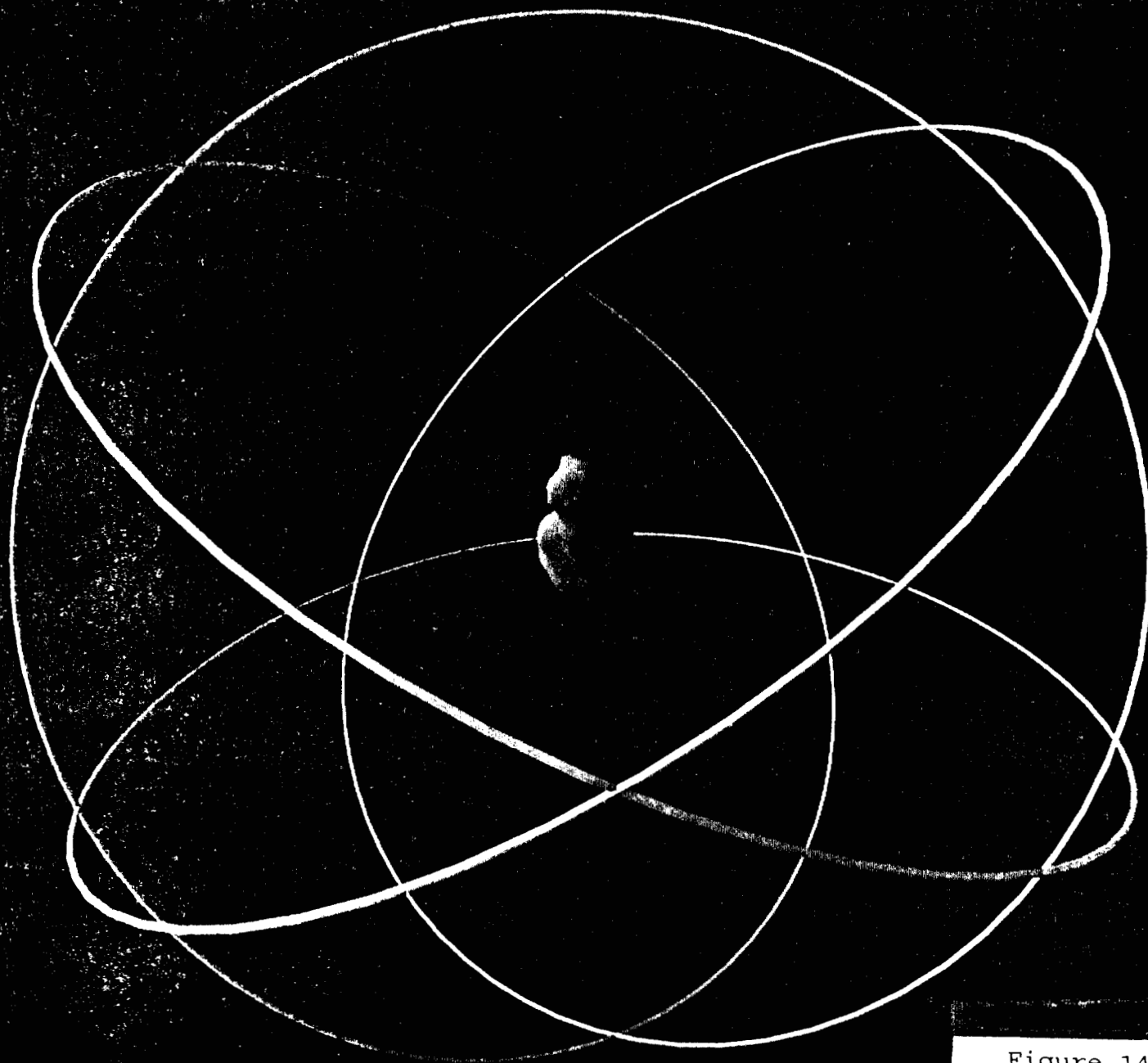
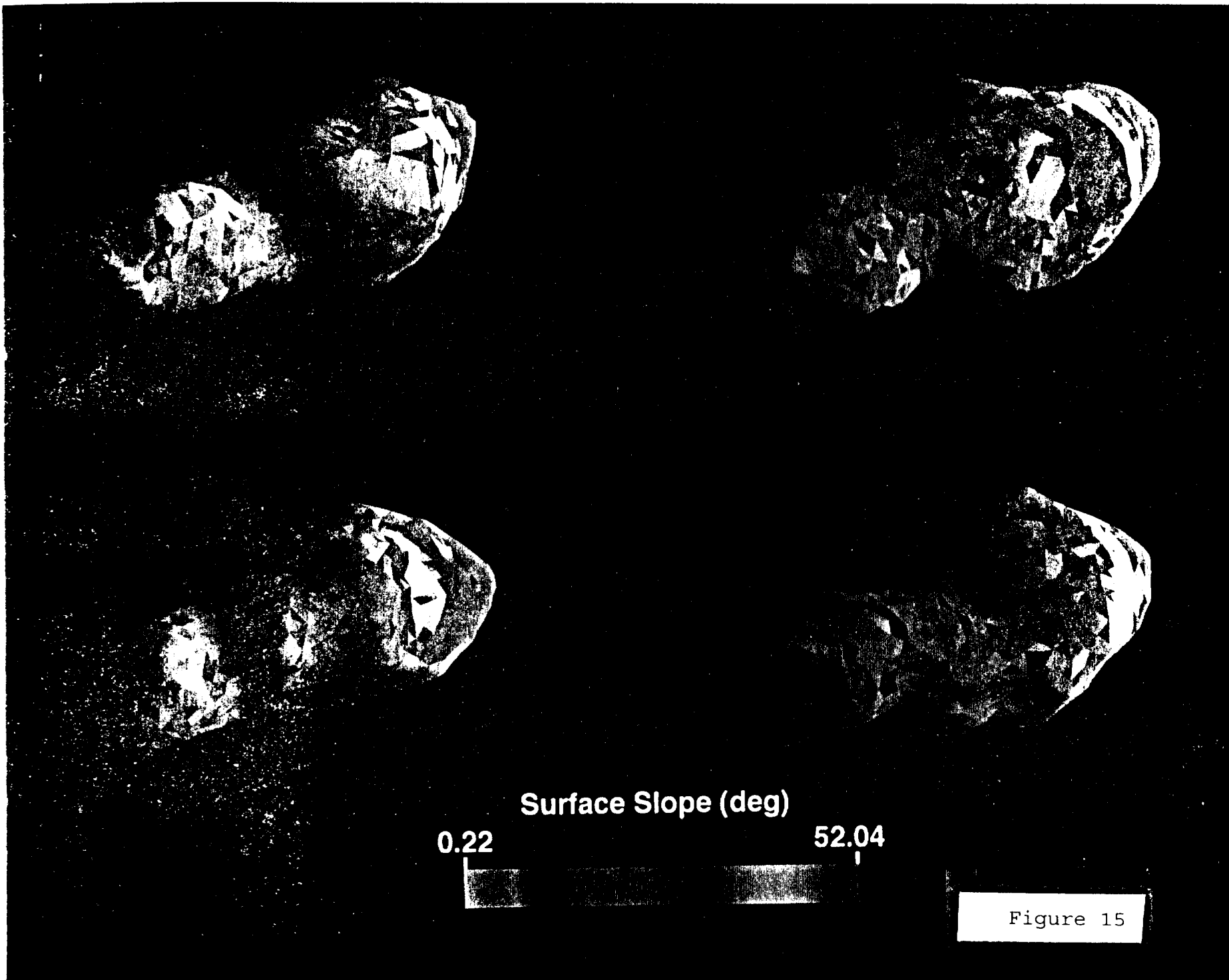


Figure 14d

Figure 14: Periodic orbits about Toutatis shown rendered in color. Shown are: a) All 1:1 Direct periodic orbits, b) One 1:1 Retrograde periodic orbit, c) One 1:2 Retrograde periodic orbits, d) One 1:3 Retrograde periodic orbit. Integrated using the full equations of motion with no approximation.



P-48744

Figure 15: Slopes over the surface of Toutatis, shown rendered in four perspective views. The viewing geometry is the same as in Figure 2. The slopes range from 0 up to 40° . The higher slopes are at the long ends of the asteroid while the smaller slopes are along the asteroid's waist. The average slope is 16° and 96% of the surface has a slope less than 35° .

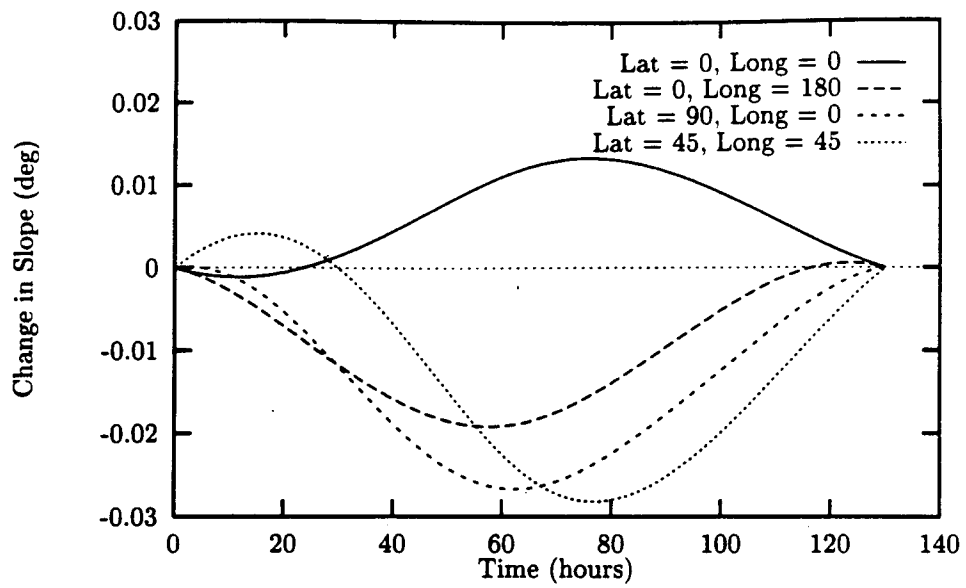


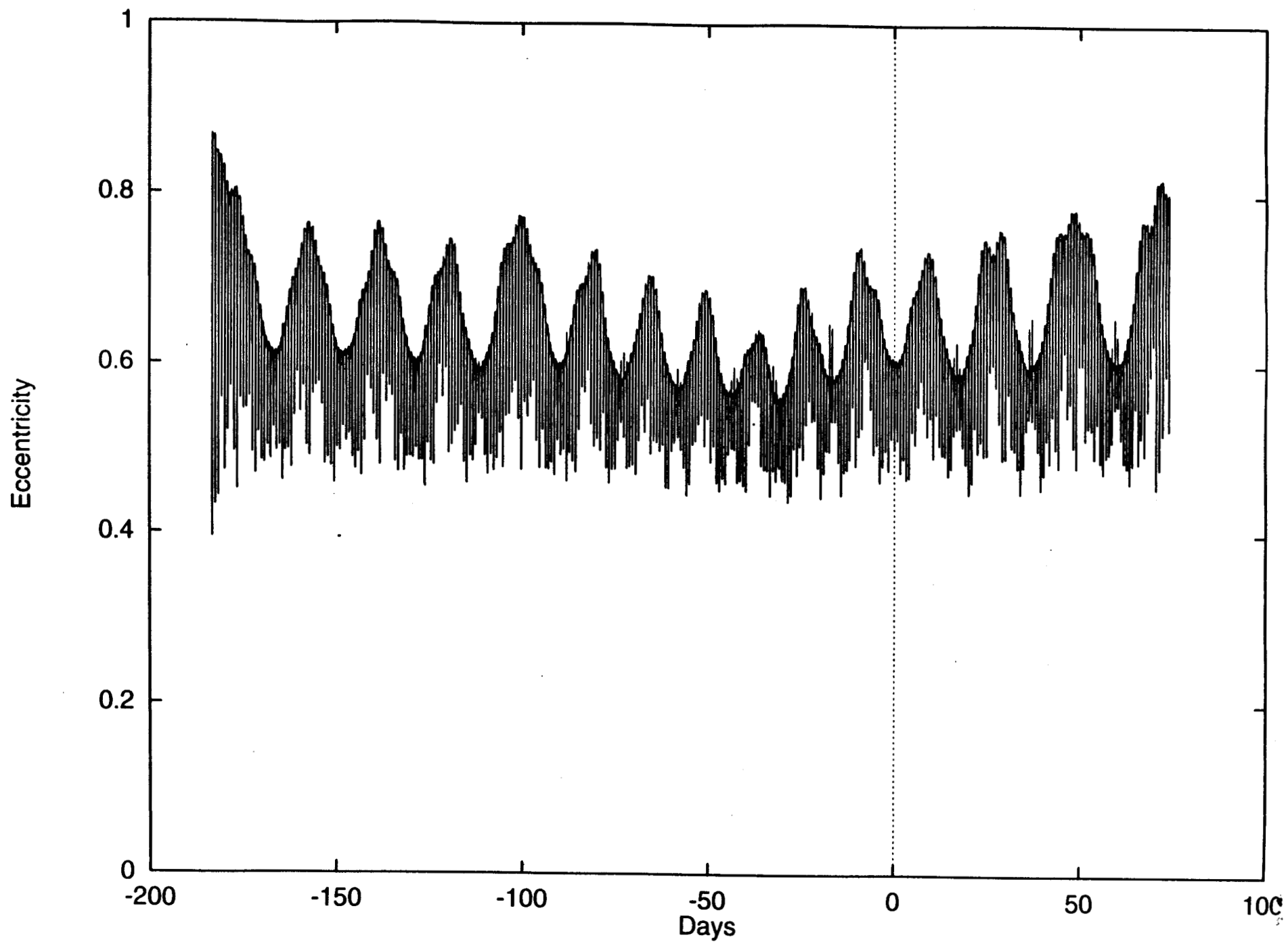
Figure 16: Variation in slope at points on Toutatis. Note that the total variation is small due to the small rotational acceleration of Toutatis. The period of the variation is fixed at 5.42 days, or 130.2 hours.



Figure 17

P-48743

Figure 17: Local normal escape speed over the Toutatis surface, shown rendered in four perspective views. The viewing geometry is the same as in Figure 2. The contribution of the angular velocity to the escape speed is small, hence the variation in these speeds are due mostly to the gravitational field of Toutatis.



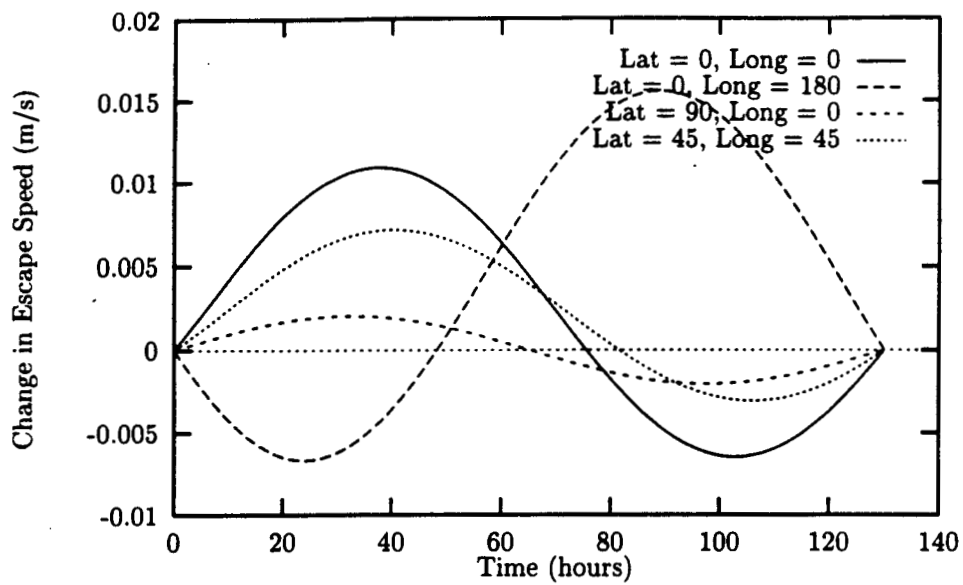


Figure 18: Change in local normal escape speed at points on Toutatis. The total variation of the escape speeds is less than a few centimeters per second, much less than this over most of the body. The period of this variation is 5.42 days or 130.2 hours.

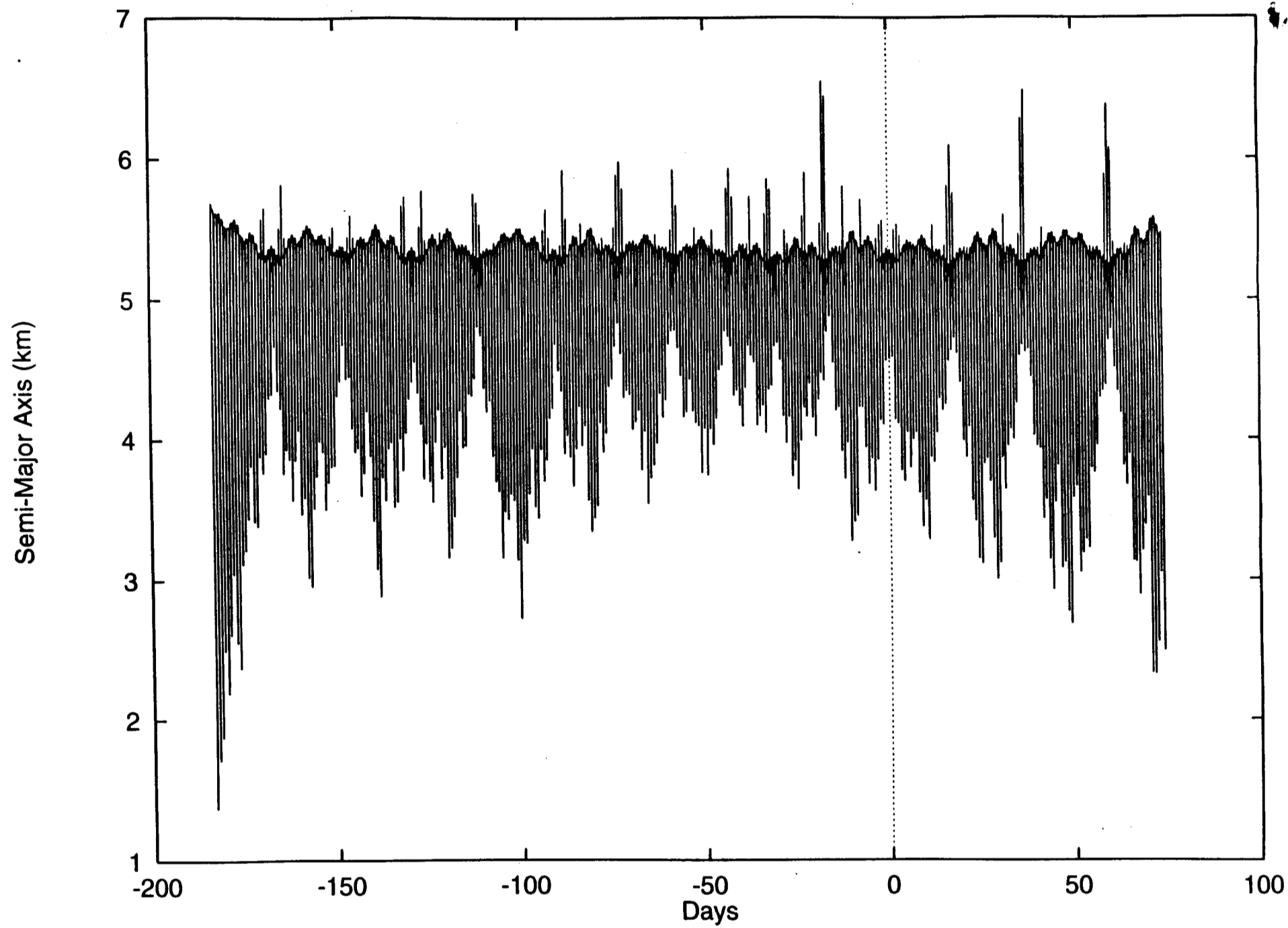


Fig 196

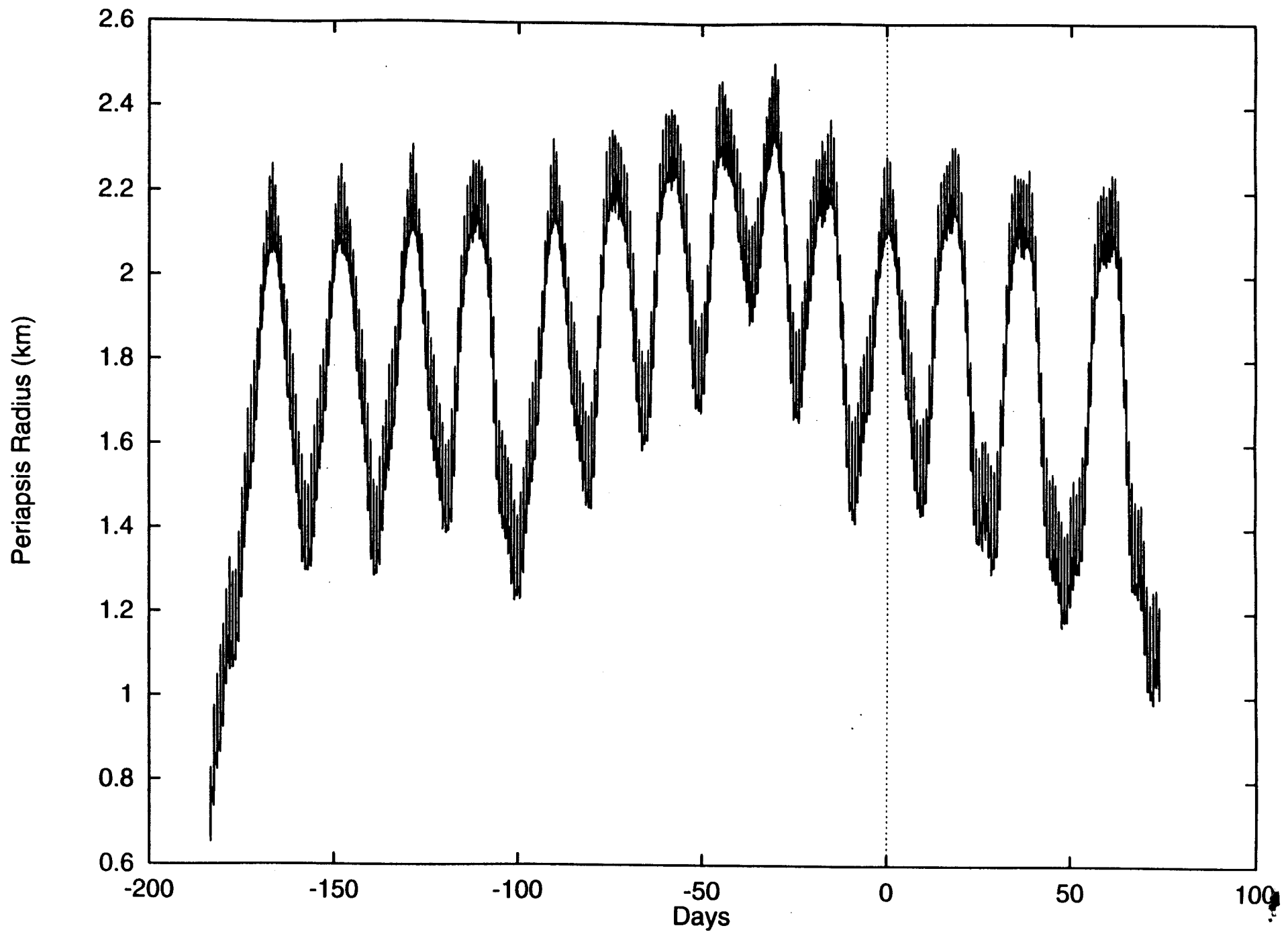


Fig 19c

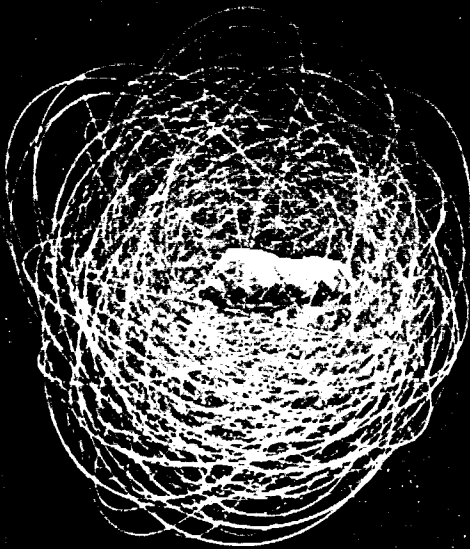
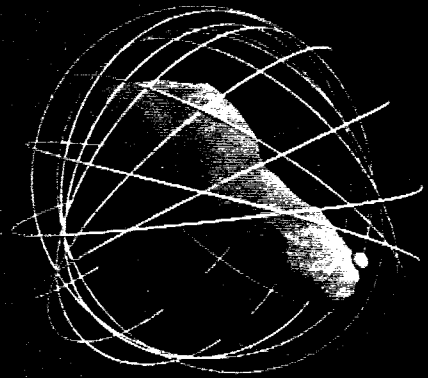
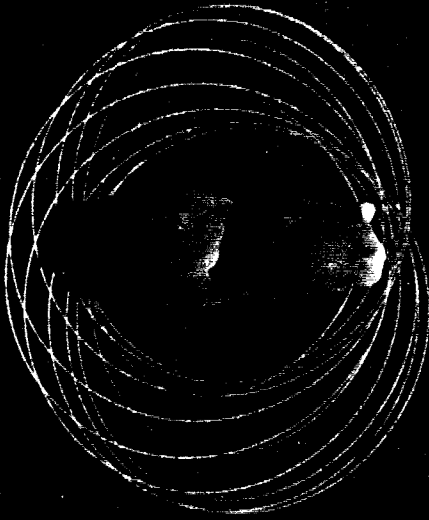
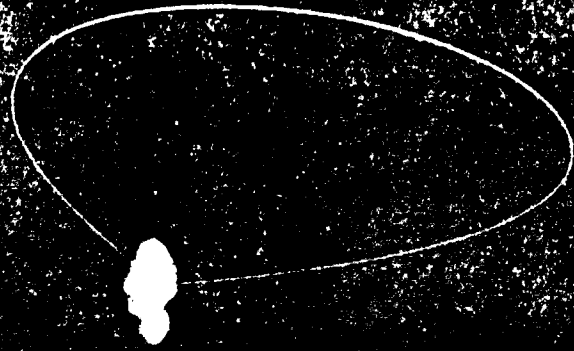


Figure 20

P-48745

Figure 20: Re-impacting ejecta orbits at Toutatis shown in body-fixed (lhs) and inertial (rhs) coordinate frames. Shown are: a) Orbit duration of 1.24 days, b) Orbit duration of 2.93 days, c) Orbit duration of 167.94 days.